PB88-250659

MIXTURE EFFECTS IN THE CATALYTIC OXIDATION OF VOC'S (VOLATILE ORGANIC COMPOUNDS) IN AIR

Research Triangle Inst.
Research Triangle Park, NC

Aug 88

U.S. Department of Commerce
National Technical Information Service
NTIS

PB88-250659

EPA/600/7-88/017
August 1988

Mixture Effects in the Catalytic Oxidation of VOCs in Air

Prepared by

S. Gangwal, K. Ramanathan, P. Caffrey,
M. Mullins, and J. Spivey
Research Triangle Institute
P.O. Box 12194
Research Triangle Park, NC 27709

EPA Cooperative Agreement CR812522
and
U.S.A.F. Interagency Agreement RN57931254

EPA Project Officer: Michael Kosusko
Air and Energy Engineering Research Laboratory
Research Triangle Park, NC 27711

AIR AND ENERGY ENGINEERING RESEARCH LABORATORY
OFFICE OF RESEARCH AND DEVELOPMENT
U.S. ENVIRONMENTAL PROTECTION AGENCY
RESEARCH TRIANGLE PARK, NC 27711

REPRODUCED BY
U.S. DEPARTMENT OF COMMERCE
NATIONAL TECHNICAL
INFORMATION SERVICE
SPRINGFIELD, VA 22161

TECHNICAL REPORT DATA
(Please read Instructions on the reverse before completing)

1. REPORT NO. EPA/600/7-88/017	2.
3. RECIPIENT'S ACCESSION NO. PB88-250659/AS	
4. TITLE AND SUBTITLE: Mixture Effects in the Catalytic Oxidation of VOCs in Air	5. REPORT DATE: August 1988
	6. PERFORMING ORGANIZATION CODE
7. AUTHOR(S): S. Gangwal, K. Ramanathan, P. Caffrey, M. Mullins, and J. Spivey	8. PERFORMING ORGANIZATION REPORT NO. 475U-3409
9. PERFORMING ORGANIZATION NAME AND ADDRESS: Research Triangle Institute, P.O. Box 12194, Research Triangle Park, North Carolina 27709	10. PROGRAM ELEMENT NO.
	11. CONTRACT/GRANT NO. EPA CR812522 and USAF IAG RN57931254*
12. SPONSORING AGENCY NAME AND ADDRESS: EPA, Office of Research and Development * Air and Energy Engineering Research Laboratory Research Triangle Park, NC 27711	13. TYPE OF REPORT AND PERIOD COVERED: Final; 6/85 - 12/87
	14. SPONSORING AGENCY CODE: EPA/600/13

15. SUPPLEMENTARY NOTES: AEERL project officer is Michael Kosusko, Mail Drop 61, 919/541-2734. (*)Cosponsor is U.S. Air Force Engineering and Services Center, Tyndall Air Force Base, FL 32403.

16. ABSTRACT

The report gives results of a study of the deep oxidation of organic mixtures over a heterogeneous catalyst in an attempt to explain earlier observations concerning the apparent inhibition or enhancement of destruction of some components to establish a scientific basis for the design and operation of catalytic incineration systems for volatile organic compound (VOC) control. To elucidate these effects, the oxidation kinetics of n-hexane, benzene, ethyl acetate, and methyl ethyl ketone (MEK) in air were examined over a commercial catalyst (0.1% Pt/3% Ni on g-alumina). Reaction rates of these components individually were determined at temperatures of 150 to 360 C from differential reactor studies. When these were compared to overall destruction efficiencies from integral reactor studies for both individual compounds and mixtures, the Mars/van Krevelen (MVK) reaction rate model satisfactorily represented the results for some single organic compounds at lower temperatures. By incorporating pore diffusion effects, the MVK model adequately explains the single component data over the entire temperature range for some of the compounds. A multicomponent MVK model incorporating competitive adsorption effects is moderately successful in predicting the observed behavior for a binary mixture of benzene and n-hexane.

17. KEY WORDS AND DOCUMENT ANALYSIS

a. DESCRIPTORS	b. IDENTIFIERS/OPEN ENDED TERMS	c. COSATI Field/Group
Pollution Organic Compounds Volatility Oxidation Catalysis Incinerators Kinetics Mathematical Models Mixtures	Pollution Control Stationary Sources Volatile Organic Compounds (VOCs) Catalytic Oxidation Mars/van Krevelen	13B 20K 07C 21C 12A 07B 07D

18. DISTRIBUTION STATEMENT: Release to Public	19. SECURITY CLASS (This Report): Unclassified	21. NO. OF PAGES: 84
	20. SECURITY CLASS (This page): Unclassified	22. PRICE: A05

EPA Form 2220-1 (9-73)

RESEARCH TRIANGLE INSTITUTE

Process Research Program

AEERL-432
Fig. 4-1 (pg 16)

November 18, 1986

Mr. William Cary
Marcel Dekker, Inc.
270 Madison Avenue
New York, NY 10016

Dear Mr. Cary:

On October 14, 1986, on the attached letter, we were granted permission to use a figure from one of your journals in a paper.

Our sponsors, the U.S. EPA would like to publish this paper as an EPA report and a NTIS report and to sell it as a NTIS report.

Details are as follows:

Journal:	Catal. Rev. - Sci. Eng.
Reference:	26(1), 1-58 (1984).
Page:	No. 5.
Figure:	No. 2

Awaiting your early consent.

Yours sincerely,

Philip R Caffrey

Philip R. Caffrey

PRC:vdw

PERMISSION GRANTED with the understanding that proper credit be given to Marcel Dekker, Inc.
References List should include:
Author's name(s), TITLE OF BOOK OR JOURNAL,
Volume____, Number____, Marcel Dekker, Inc., N.Y.
Year of Publication
Each item to be reprinted should carry the lines
. . . . . 1, p. _____, by

Ellen Lynch 12/9/80

Post Office Box 12194 Research Triangle Park, North Carolina 27709 Telephone: 919 541-6000

1a

OK

NOTICE

This document has been reviewed in accordance with U.S. Environmental Protection Agency policy and approved for publication. Mention of trade names or commercial products does not constitute endorsement or recommendation for use.

TABLE OF CONTENTS

Section		Page
1.0	Executive Summary	1
2.0	Introduction	2
3.0	Experimental	7
4.0	Results	15
5.0	Development of a Reactor Model for Predicting Deep Oxidation Behavior of Hydrocarbon Mixtures	31
6.0	Autocatalysis in Deep Oxidation of Ethyl Acetate	62
7.0	Conclusions and Recommendations	68
8.0	Data Quality	69
9.0	Nomenclature	73
10.0	References	76

LIST OF FIGURES

Number		Page
3-1.	Microreactor system	10
3-2.	Sequential analysis of reactor inlet (bypass) and reactor outlet with a 10-port "zero" volume valve	12
4-1.	Rate controlling regimes in a catalytic combustor	16
4-2.	Effect of multicomponent mixtures on n-hexane conversion	17
4-3.	Effect of multicomponent mixtures on benzene conversion	18
4-4.	Effect of multicomponent mixtures on ethyl acetate conversion	19
4-5.	Effect of multicomponent mixtures on MEK conversion	20
4-6.	Comparison of the effect of benzene on ethyl acetate and MEK conversion	22
4-7.	First order rate constants for the oxidation of single components	24
4-8.	First order rate constants for oxidation in a ternary mixture	25
4-9.	Differential reaction rate for n-hexane oxidation	27
4-10.	Differential reaction rate for benzene oxidation	28
4-11.	Differential reaction rate for ethyl acetate oxidation	29
4-12.	Differential reaction rate for MEK oxidation	30
5-1.	Inverse reaction rate versus inverse concentration for n-hexane oxidation	33
5-2.	Inverse reaction rate versus inverse concentration for ethyl acetate oxidation	34
5-3.	Inverse reaction rate versus inverse concentration for MEK oxidation	35
5-4.	Mars/van Krevelen rate constants for n-hexane oxidation	37
5-5.	Mars/van Krevelen rate constants for ethyl acetate	38
5-6.	Mars/van Krevelen rate constants for MEK oxidation	39
5-7.	Mars/van Krevelen rate constants for benzene oxidation	40

5-8. Comparison of predicted and actual conversions for benzene and n-hexane in a binary mixture.....49

5-9. Comparison of predicted and actual conversions for ethyl acetate and n-hexane in a binary mixture.....50

5-10. Evaluation of collision integral for modeling purposes in the temperature range of interest.....55

5-11. Comparison of model predictions and experimental data for n-hexane conversion as a single component.....57

5-12. Comparison of model predictions and experimental data for benzene conversion as a single component.....58

5-13. Comparison of model predictions and experimental data for binary benzene/n-hexane mixture.....59

5-14. Comparison of model predictions and experimental data for ethyl acetate conversion as a single component.....60

6-1. Comparison of ethyl acetate conversions in dry and humidified air streams.....64

6-2. Comparison of MEK conversions in dry and humidified air streams.....67

LIST OF TABLES

Number — Page

2-1. Approximate range of independent variables for this research..... 4

3-1. Test gas mixtures..... 8

3-2 Catalyst characteristics..... 9

3-3. Experimental conditions.....14

5-1. Mars/van Krevelen rate equation parameters.....41

5-2. Multicomponent oxidation model with internal diffusion.....46

5-3. Multicomponent oxidation model in non-dimensional form.....47

5-4. Catalyst physical properties for modeling and $D_{eff(i)}$ calculation.....52

8-1. Precision of data.....70

8-2. Accuracy of data.....72

1.0 EXECUTIVE SUMMARY

Most volatile organic compound (VOC) releases into the environment are mixtures, and rarely consist of a single component. However, the bulk of fundamental studies of the catalytic deep oxidation of such compounds are usually confined to single components. This study examines the deep oxidation of organic mixtures over a heterogeneous catalyst in an attempt to explain earlier observations by Tichenor, et al.(1987) concerning the apparent inhibition or enhancement of oxidation of some components to establish a scientific basis for the design and operation of catalytic incineration systems for VOC control. To elucidate these effects, the oxidation kinetics of n-hexane, benzene, ethyl acetate, and methyl ethyl ketone in air were examined over a commercial catalyst (0.1 percent Pt/ 3 percent Ni on γ-alumina.) Reaction rates of these components individually were determined at temperatures of 150°C to 360°C from differential reactor studies. When these were compared to overall destruction efficiencies from integral reactor studies for both individual compounds and mixtures, the Mars/van Krevelen (MVK) reaction rate model satisfactorily represented the results for some single organic compounds at lower temperatures. By incorporating pore diffusion effects, the MVK model adequately explains the single component data over the entire temperature range for some of the compounds. A multicomponent MVK model incorporating competitive adsorption effects is moderately successful in predicting the observed behavior for a binary mixture of benzene and n-hexane; however, this model can not predict the apparently enhanced reaction rate observed for ethyl acetate at higher temperatures (>220°C). Other reaction pathways available for compounds with carbon-oxygen linkages and/or the advent of catalytically supported homogeneous combustion with free radical precursors may explain this phenomenon. The enhancement of ethyl acetate conversions in humidified air streams suggests that autocatalysis by product water may be a possible mechanism.

2.0 INTRODUCTION

The goal of this Cooperative Agreement is to establish a scientific basis for the selection and evaluation of heterogeneous catalysts and operating conditions for the control of gas streams containing mixtures of volatile organic compounds (VOCs). The research has been devoted to both experimental evaluation of the catalytic oxidation of VOC-containing mixtures and to the kinetic interpretation/modeling of the results.

Heterogeneous catalytic oxidation of organic compounds is an important and intensely studied area. Much research has been reported on industrially important partial oxidation reactions and catalytic oxidation of automotive exhaust. Catalytic oxidation is often used instead of direct thermal oxidation for control of VOC emissions from a number of sources due to its lower operating temperature which results in lower NO_x emissions and lower operating cost (primarily due to lower fuel consumption). However, fundamental studies of the behavior of complex and sometimes incompletely characterized mixtures of VOCs from operations such as air stripping of contaminated groundwater are relatively scarce. It is the purpose of this Cooperative Agreement to address this need.

Of particular interest is the interaction of one VOC with others in a multicomponent gas phase mixture. As such a mixture passes over a catalyst designed to achieve some level of environmental control, this interaction has extremely practical implications. For example, in the oxidation of chlorinated VOCs, it is possible in principle to produce a gas with higher toxicity than the inlet gas by incomplete oxidation of the VOC. Also of interest are the relative interactions of classes of VOCs that might be encountered in environmental control situations. For instance, if some generalization could be made that aromatics usually enhance the oxidation of ketones, or that the presence of chlorinated solvents usually inhibits the oxidation of alkanes but not esters, this would allow the Agency or the U.S. Air Force to make some preliminary judgements when faced with the problem of controlling VOC-

containing gas streams. It is likely that any such generalizations would be highly dependent on the catalyst and reaction conditions. While it is not within the scope of this research to characterize the behavior of all likely VOCs on all applicable catalysts at all typical conditions, we hope to describe quantitatively, through experiments and kinetic modeling, the behavior of a few well-defined VOC mixtures containing different classes of compounds. Experimental conditions are shown in Table 2-1. We have taken care in selecting these compounds, catalysts, and reaction conditions to help ensure that the results are of the most direct use for the Agency and the U.S. Air Force.

From the literature pertinent to this study (Spivey, 1987), several conclusions can be drawn:

- Catalysts which have been shown to be effective for VOC control at the conditions of Table 2-1 include supported noble metals (primarily Pt, with and without base metal oxides such as NiO), single metal oxides (e.g., Cr_2O_3 or V_2O_5) and mixed metal oxides (e.g., hopcalite). As a very general rule, supported noble metals are more active, more easily poisoned (especially by halogenated VOCs), and more widely used.

- Applications of catalytic oxidation for VOC control have primarily involved direct transfer of technology from related applications, such as the use of an automotive catalyst downstream of a burner. Little has been done to develop catalysts specifically for this need.

- The use of catalytic oxidation as a VOC control technique is more widespread in Europe than in the United States, perhaps because of higher energy costs and more stringent environmental regulations (Acres, 1970).

- Very little has been reported on the systematic scientific study of VOC mixtures. Reported work tends to be either well characterized research on pure components in air or anecdotal studies of "real" streams where only gross performance is reported.

TABLE 2-1. APPROXIMATE RANGE OF INDEPENDENT VARIABLES FOR THIS RESEARCH

Temperature	150 - 400°C
Pressure	1 atm
Space velocity	10^4 - 10^6 hr^{-1}
Reactant concentration	10^1 - 10^3 ppm
Reactants	Chlorinated solvents, alkanes, aromatics, and oxygenated hydrocarbons (ketones, acetates, esters)
Humidities	0 - 80% RH
Oxidant	Air

- Modeling of the catalytic oxidation of VOCs at conditions of interest may be complex, especially for mixtures, because of both surface kinetic and mass transfer effects that can vary with experimental conditions. These effects may result in inhibition or enhancement of the oxidation of a given compound.

Most research on catalytic oxidation of VOCs tends to involve either single pure components, with relatively complete analysis of reaction products, or field studies, with only the overall performance (e.g., "percent removal") being reported. From the relatively few systematic studies of mixture effects in catalytic oxidation of VOCs, several conclusions can be drawn.

Though some evidence exists that partial catalytic oxidation of mixtures of closely related compounds can be predicted directly and linearly from single component behavior (Emmett, 1960), most studies show inhibition of the oxidation of one or all of the compounds in a mixture over their behavior as single components. Satterfield (1980) states that this inhibition can be accounted for by competition among the reactants (VOCs in this case) for adsorption sites on the catalyst. Yao (1973), in studying primarily C_2 and C_3 hydrocarbons over α-Cr_2O_3 further suggests that the observed inhibition in hydrocarbon mixtures can be explained by competition among the hydrocarbons for adsorbed O_2 or for undefined "adsorption sites" (presumably lattice oxygen from the α-Cr_2O_3).

Cullis et al. (1970) found another type of mixture effect in studying methane oxidation over Pd catalysts. Propane, when added to methane, significantly retarded methane oxidation but was itself oxidized very little. Perhaps some trace level of a compound generated by the oxidation of a very small amount of propane was sufficient to retard methane oxidation. A similar effect might take place in a VOC mixture.

Much work out of the Warren Springs Lab in England (Pope et al. 1976 and 1978; Heyes et al. 1982) has examined the catalytic oxidation of hydrocarbons in mixtures with sulfur-containing species on some single metal oxides and supported Pt. The general conclusion from this work is that the sulfur-containing compounds suppressed hydrocarbon oxidation and that small concentrations of products of incomplete combustion were almost always observed, though not identified.

Tichenor and Palazzolo (1987) also studied mixture effects and observed enhancement, inhibition, and no effect on some VOCs in mixtures compared to their oxidation as single components. They also identified quite a number of the incomplete combustion products.

The conclusion from these studies can be no more specific than that mixture effects are typically observed and, at least to date, are fairly unpredictable. It is the goal of this research to extend the current understanding.

3.0 EXPERIMENTAL

3.1 Chemicals

Benzene, n-hexane, ethyl acetate, and methyl ethyl ketone (MEK) were chosen for this study as representing the classes of aromatic, aliphatic and oxygenated species respectively. The gases were obtained premixed with hydrocarbon free, dry air in gas cylinders at concentrations ranging from 10 to 600 ppmv hydrocarbon from Scott Specialty Gases, Plumsteadville, PA. A number of gases containing single components, binary mixtures, and ternary mixtures were obtained as shown in Table 3-1. The gases were used one at a time in the deep-oxidation experiments.

3.2 Catalysts

The catalyst was obtained from United Catalyst, Inc., Louisville, KY, as 1/4-in. (6.35 mm) cylinders. The commercial designation of the catalyst was G-43, and its nominal composition as supplied by the vendor was 0.1 percent Pt, 3 percent Ni/γ-Al_2O_3. The catalyst was crushed and screened to 120 x 170 mesh prior to use in the oxidation experiments. The physical properties of the catalyst, as specified by the vendor and as measured in RTI's laboratory, are given in Table 3-2.

3.3 Apparatus

A laboratory-scale microreactor system, shown in Figure 3-1, was used for all the experiments. The reactor consisted of a 60-cm-long Pyrex tube (6 mm O.D., 4 mm I.D. for the 60 x 80 mesh catalyst; 3 mm O.D., 1.5 mm I.D. for the 120 x 170 mesh catalyst), and the catalyst was positioned at the center of the tube using fine Pyrex wool plugs. The tube was surrounded by a three-zone 45-cm-long split tube furnace. The end zones were each 7.5-cm-long and the central zone was 30-cm-long. The temperature of each heating zone was controlled separately using proportional temperature controllers. A single zone furnace was used for the experiments involving MEK, which were carried out after a redesign of the experimental setup. Four 0.5-mm O.D. measurement

TABLE 3-1. TEST GAS MIXTURES

	Concentration in Air (ppmv)
Single Hydrocarbon	benzene: 9, 69, 163, 375, 525 ethyl acetate: 53, 109, 238, 450 n-hexane: 201, 410, 566 methyl ethyl ketone (MEK): 25, 50, 70 135, 190, 298
Binary Mixtures	193 ppm benzene + 172 ppm ethyl acetate 189 ppm benzene + 190 ppm n-hexane 184 ppm ethyl acetate + 190 ppm n-hexane 149 ppm n-hexane + 135 ppm MEK 160 ppm benzene + 135 ppm MEK
Ternary Mixtures	143 ppm benzene + 174 ppm ethyl acetate + 90 ppm n-hexane; 103 ppm n-hexane + 104 ppm benzene + 93 ppm MEK

TABLE 3-2. CATALYST CHARACTERISTICS

Vendor	Measured
Composition: 0.1% Pt, 3% Ni/γ-Al_2O_3	3.18% Ni, 48.2% Al, 46.3% Oxygen*
Form: 1/4-in. (6.35 mm) extrudates (crushed to 120 x 170 mesh and 60 x 80 mesh prior to use)	
BET Surface Area: 212 m^2/g	161 m^2/g
Pore Volume:	
0-150 nm (Nitrogen BET Method)	0.364 cm^3/g
1.4 to 14 nm (CCl_4 Method): 0.26 cm^3/g	
1.4 to 80 nm (CCl_4 Method): 0.28 cm^3/g	
Mean Pore Radius (estimated)	3.6 nm
Particle Density	1.46 g/cm^3
Pore Volume Distribution (Mercury Porosimetry, 60,000 psi [414 MPa]):	
175 to 12um 0.00 cm^3/g	
12 um to 80 nm 0.08 cm^3/g	
80 to 14 nm 0.01 cm^3/g	
14 to 2.9 nm 0.23 cm^3/g	

* Pt below detection limit of ESCA [electron spectroscopy for chemical analysis]

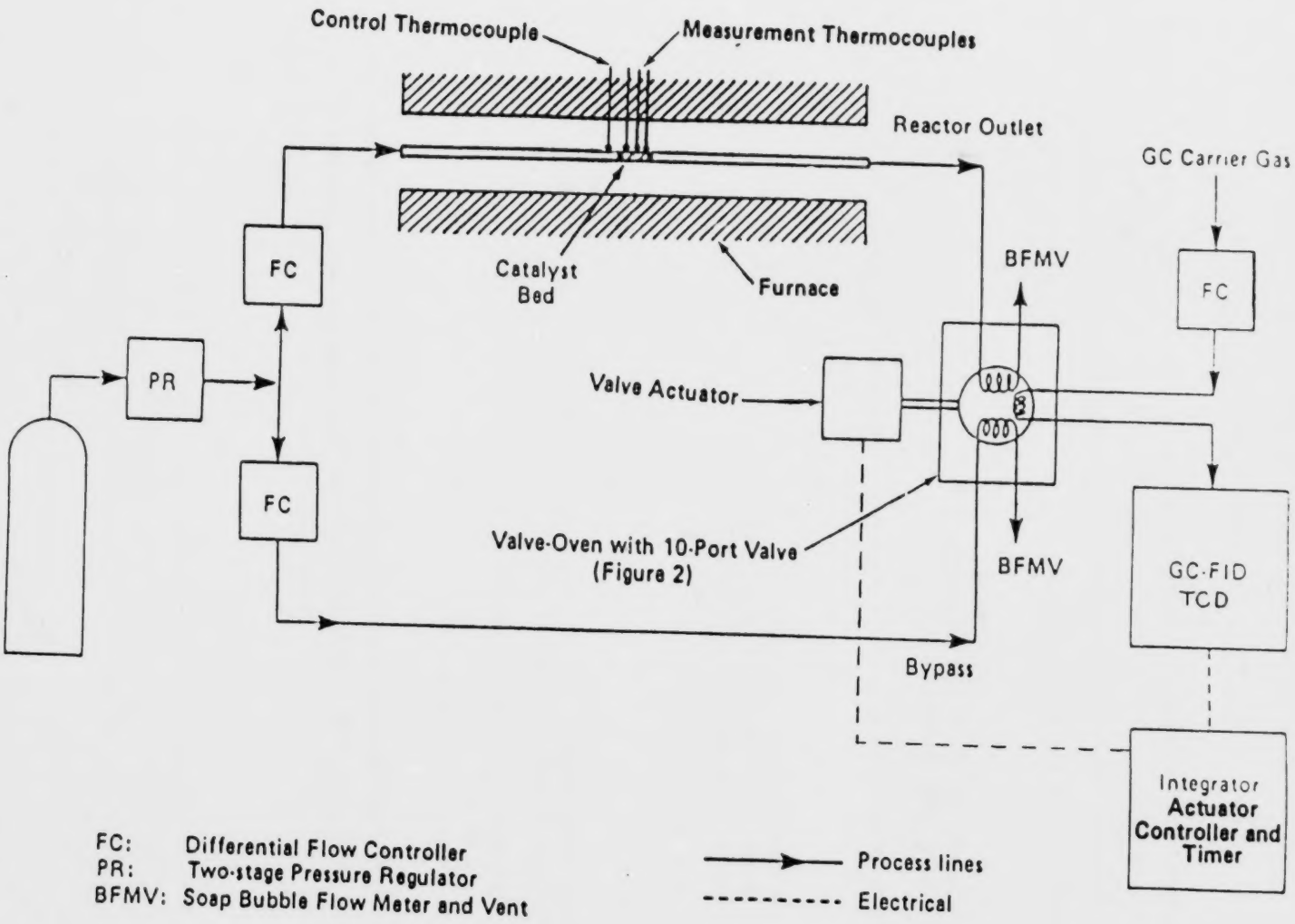

Figure 3-1 . Microreactor system.

thermocouples (type K) were mounted, equally spaced, along the small catalyst bed to ensure temperature uniformity. The temperature control was better than ±0.5°C in each zone. The premixed gas was delivered using a two-stage pressure regulator with the gas-flow split into two equal flows using two differential flow controllers as shown. One flow stream was passed through the microreactor, whereas the other was passed through a bypass line. After the two split gas streams flowed through the reactor and the bypass line respectively, they entered a thermostatted Valco 10-port gas sampling valve maintained at 100°C. The 10-port valve is a unique device that allows sequential sampling of the reactor outlet stream and the bypass stream (i.e., representative of the reactor inlet stream) using two identical 0.25-cm^3 sample loops.

Sequential sampling using this valve is illustrated in Figure 3-2. The samples were injected automatically, using a Carle Valve Minder consisting of a valve actuator and a valve timer, into a Varian 3700 gas chromatograph (GC) equipped with a flame-ionization detector (FID). A 5 ft (1.5 m) long, 1/8-in. (3 mm) stainless-steel column consisting of 3 percent SP 1500 on 80/120 mesh Carbopack B was used for the separation and analysis of the hydrocarbons isothermally at 140°C. A Carle 111 GC with an FID was used in the later experiments. A complete analysis of the three hydrocarbons of interest could be performed in 4-1/2 minutes. The valve timer was placed on a 9-minute cycle to allow the measurement of the hydrocarbons in the reactor inlet and in the reactor outlet streams sequentially. Because the inlet concentration of the gas stream was a known constant, the outlet concentration was obtained assuming a linear response of the FID with respect to the inlet concentration for the hydrocarbons of interest. The analysis of the inlet during every cycle is extremely important because of variation of the FID response during the course of a typical day of the experiment. Even though the FID response may drift or cycle during the day, it would affect the outlet and the inlet stream concentrations in a fixed ratio. Thus, the sampling procedure allowed accurate measurement of the reactor outlet concentrations, irrespective of the drift in the FID response. The peak areas were measured electronically using a Perkin-Elmer Sigma 10B Data Station. This data station was also used to time the automatic injections in the later experiments. The bypass and reactor outlet gas flows were measured using a soap bubble flow meter to

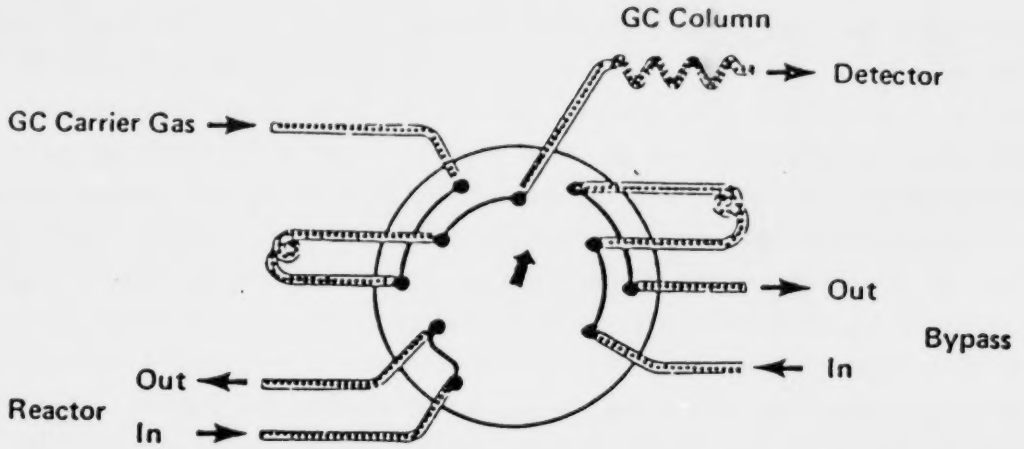

Valve Position A: Analyze reactor outlet

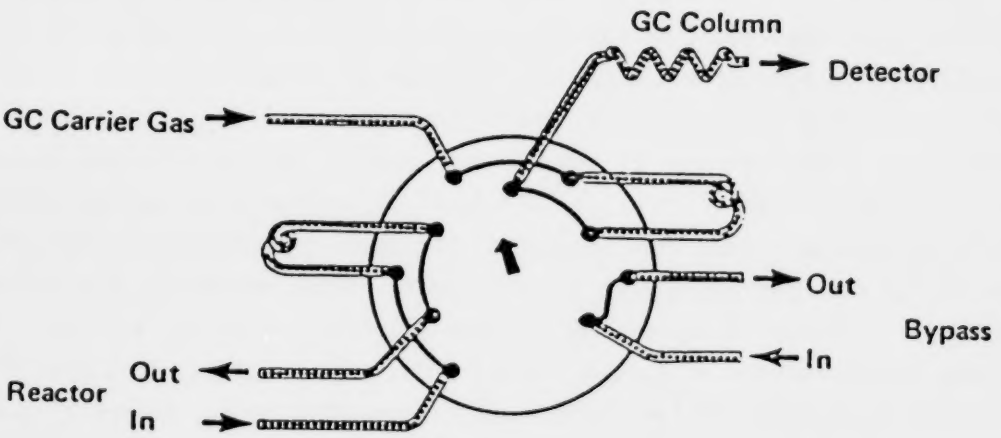

Valve Position B: Analyze reactor inlet (bypass)

Figure 3-2. Sequential analysis of reactor inlet (bypass) and reactor outlet gases with a 10-port "zero" volume valve.

ensure that they were equal. This equality of flow was necessary for accurate determination of the reactor outlet concentration.

3.4 Procedure

Typical experimental conditions (including reactor size, catalyst particle size, temperature range, pressure, and space velocities) are shown in Table 3-3. The experimental procedure consisted of measuring the reactor inlet and outlet concentrations at a series of constant temperatures and gas flow rates for each gas. Integral reactor high-conversion experiments were carried out initially. Single-component gases were run first, followed by the binary mixtures and the ternary mixture. These experiments allowed gross evaluations of the regimes of surface reaction, pore diffusion, external diffusion, and catalytically supported thermal reaction. These experiments also allowed us to establish whether or not mixture effects were present to a significant degree. More fundamental differential reactor experiments (less than 10 percent conversion) were then carried out for each pure component in the surface reaction controlled region to evaluate its rate expression. These rate expressions are used to explain the results of the integral reactor experiments and to evaluate mixture effects.

TABLE 3-3. EXPERIMENTAL CONDITIONS

Pressure:	Atmospheric
Temperature Range:	140 to 360°C (isothermal operation)
Space Velocity at Reaction Temperature:	50,000 to 1,000,000 h^{-1}
Catalyst Bed:	17 to 20 mg
Hydrocarbon Concentration in Air:	10 to 600 ppmv
Catalyst Particle Size:	120 to 170 mesh
Ratio of Reactor Diameter to Particle Diameter	20:1

4.0 RESULTS

During initial exposure of the 0.1-percent Pt, 3-percent Ni/γ-Al_2O_3 catalyst to an air stream containing n-hexane at approximately 315°C, the catalyst exhibited a prolonged induction period (up to 72 hours) during which catalyst activity increased by nearly 2 orders of magnitude. Based on scanning electron microscopy/energy-dispersive x-ray analysis experiments, we believe that this induction period was caused primarily by slow redispersion of the Pt on the surface of the catalyst. The activity increased further at a higher reaction temperature of 365°C until a stable activity was reached. Once the steady-state activity was reached, it remained stable throughout the duration of the experiments. Only the steady-state results are presented.

Before presenting the results, it is instructive to consider the three operating regions of an industrial catalytic combustor as designated by Prasad et al. (1984) and shown in Figure 4-1. Generally, the inlet fuel/air mixture temperature is low, and the rate of combustion (oxidation) is controlled by intrinsic kinetics (region A). As temperature rises along the bed, the rate increases exponentially to a point where it is not possible to supply the reactant to the catalyst surface fast enough to keep up with the rate of reaction. This marks the beginning of the mass-transfer-controlled region (region B). The rate in region B may be controlled by external diffusion, internal (pore) diffusion, or a combination of both, depending on hydrodynamic conditions and catalyst physical structure. Farther downstream in the bed, the exothermic oxidation reactions increase the temperature to a point where gas-phase reactions begin to occur simultaneously with the catalytic reactions. This region is designated as the catalytically supported homogeneous reaction region (region C), where the rate again increases exponentially.

Figures 4-2 through 4-5 show the conversion data for n-hexane, benzene, ethyl acetate and methyl ethyl ketone (MEK) as a function of temperature in various mixtures. All these results were obtained at an identical weight

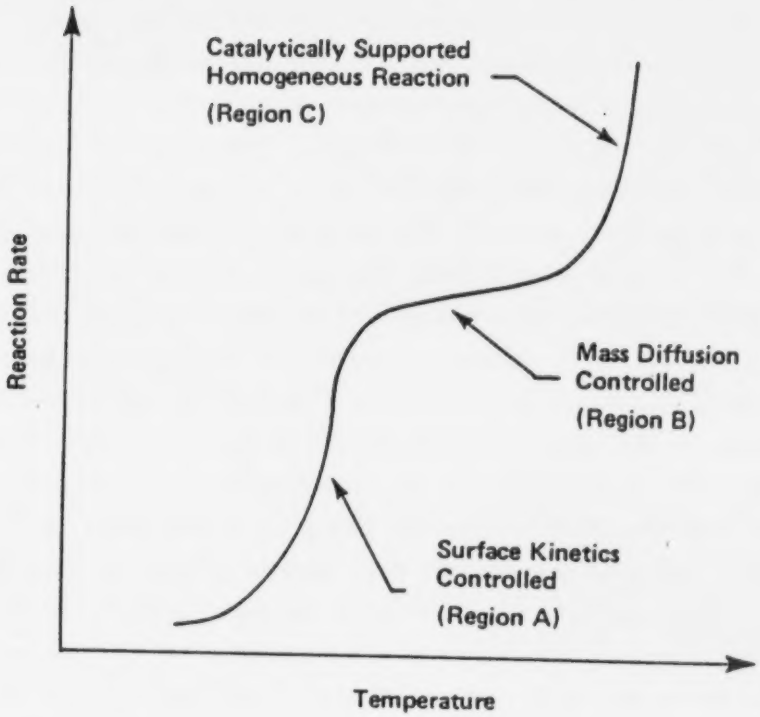

After Prasad et al. (1984)

Figure 4-1. Rate controlling regimes in a catalytic combustor.
(reproduced with permission from Marcel Dekker, Inc., N.Y., N.Y.)

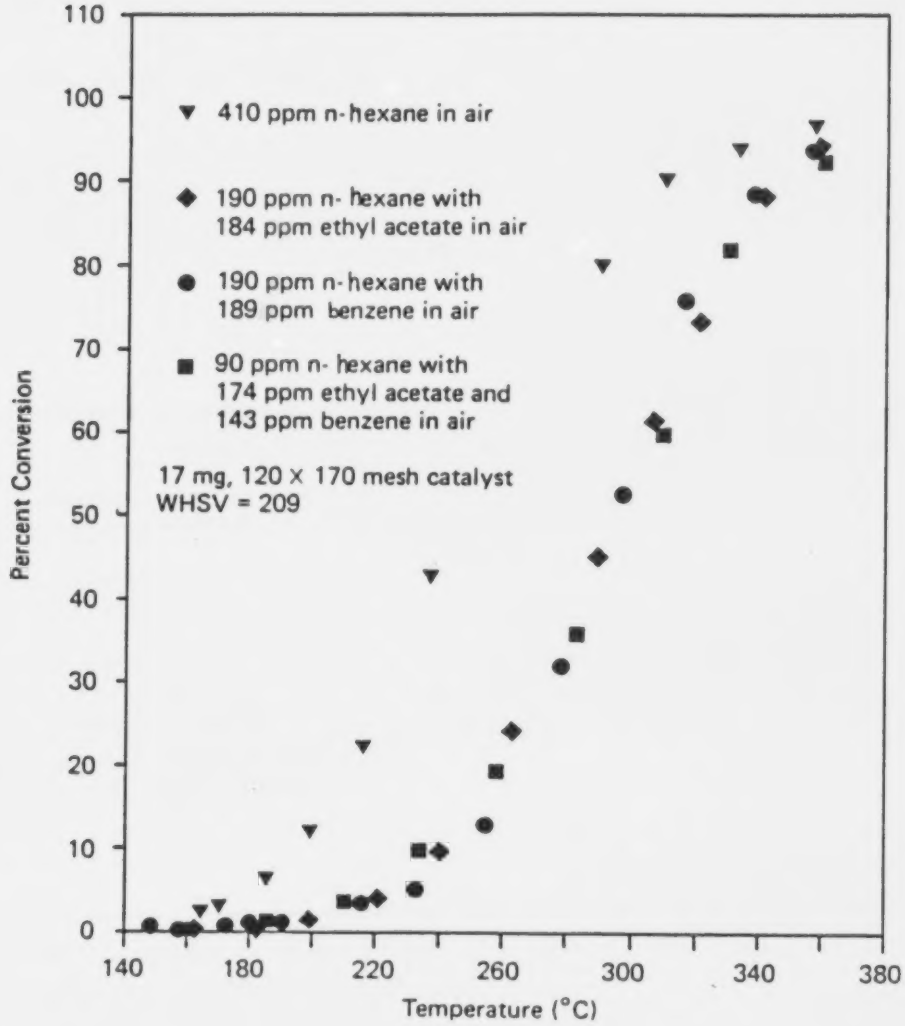

Figure 4-2. Effect of multicomponent mixtures on n-hexane conversion.

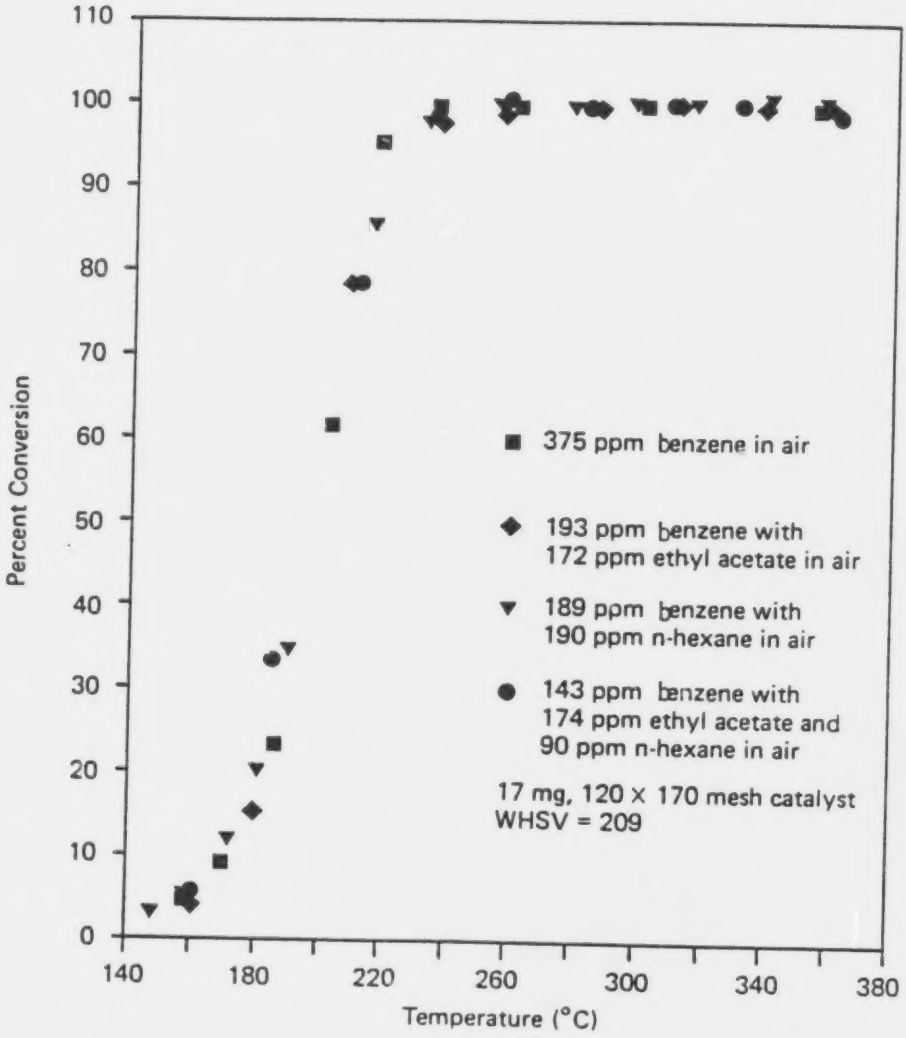

Figure 4-3. Effect of multicomponent mixtures on benzene conversion.

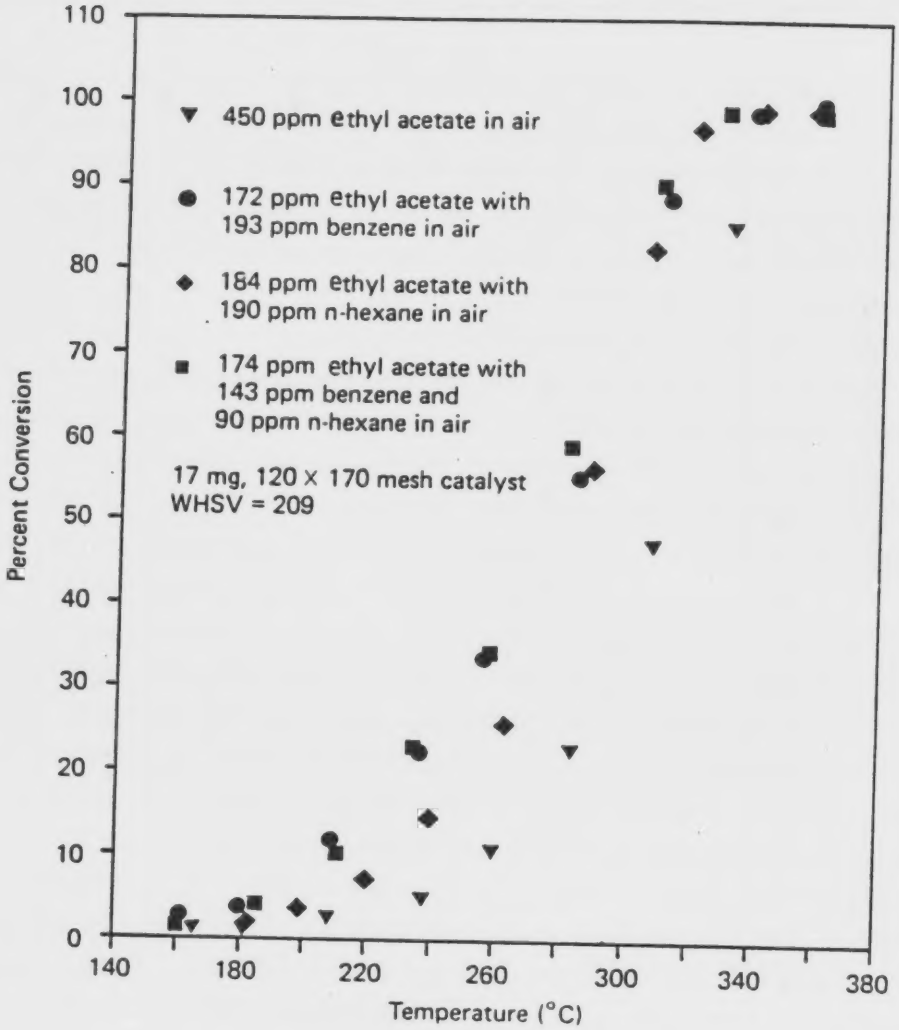

Figure 4-4. Effect of multicomponent mixtures on ethyl acetate conversion.

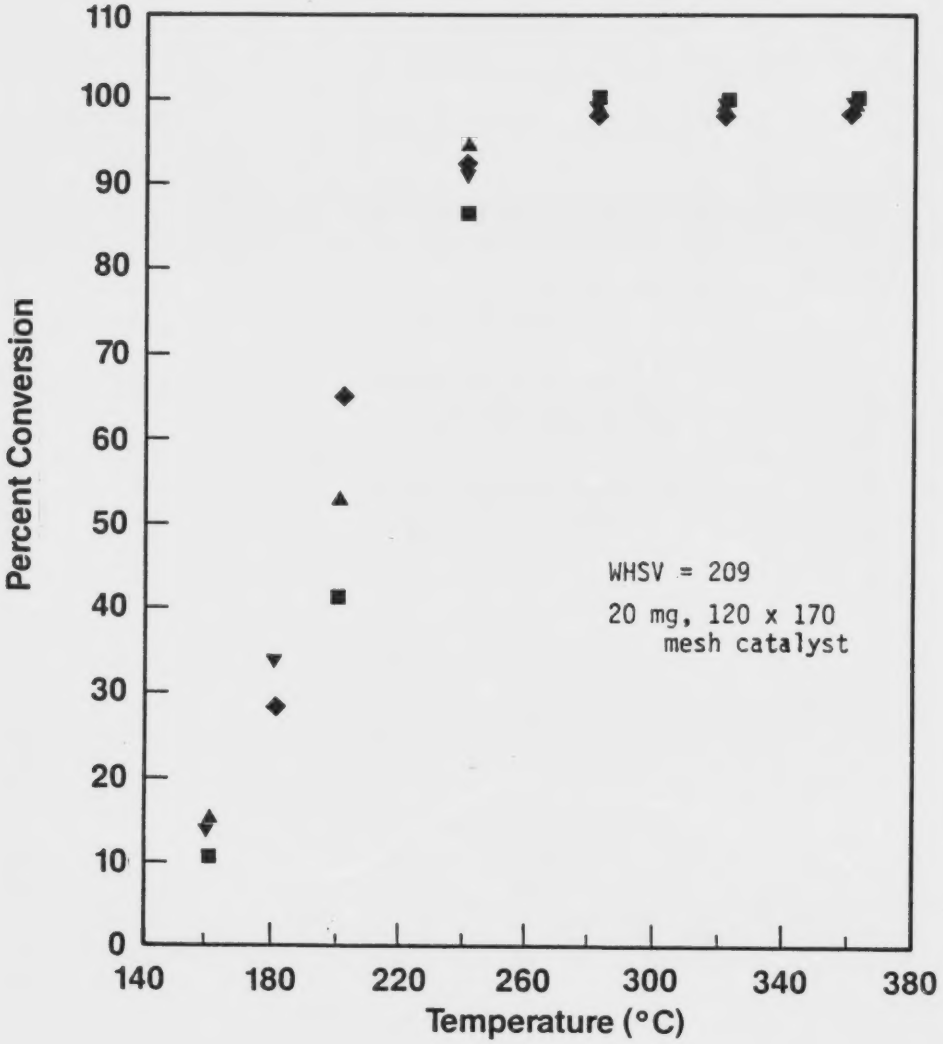

■ 297 ppm MEK in air
◆ 135 ppm MEK and 160 ppm benzene in air
▲ 135 ppm MEK and 149 ppm hexane in air
▼ 93 ppm MEK, 103 ppm n-hexane and 104 ppm benzene in air

Figure 4-5. Effect of multicomponent mixtures on MEK conversion.

hourly space velocity (WHSV) of 209, where WHSV is defined as the weight of the flowing gas per unit weight of catalyst per hour. A direct comparison of these figures with Figure 4-1 is not possible because the abscissas are percent conversion in one case and reaction rate in the other. Direct conclusions regarding the operating regions of our data is thus not possible without measurement of reaction rates.

As shown in Figure 4-2, the conversion of n-hexane is significantly inhibited in mixtures versus as a single component. The inhibition at low temperatures (<260°C) is highest in the presence of benzene. From Figure 4-3, the conversion of benzene appears to be nearly unaffected in the mixtures. From Figure 4-4, the conversion of ethyl acetate is significantly enhanced in the mixtures. (Enhancement is highest in the mixtures containing benzene). These observations confirm those of Tichenor and Palazzolo (1987). The enhancement of ethyl acetate conversion led to the selection of another oxygenated species, MEK, for mixture studies in order to see if enhancement was a trend for oxygenated species. From Figure 4-5, MEK conversion is enhanced but not as much as ethyl acetate. The pure compound reactivity of MEK is comparable to benzene. Figure 4-6 compares mixture effects of ethyl acetate and MEK in binary mixtures with benzene.

As pointed out earlier, all data in Figures 4-2 through 4-5 are at the same space velocity. Another way to present the data would be in terms of reaction-rate constants, which allows data at different space velocities to be represented concisely as shown in Equation (1) below. For deep oxidation of trace organics, the most popular assumption in the literature for kinetics is first order in terms of the organic concentration (Hawthorn, 1974; Morooka et al., 1967; Sadamori et al., 1981; Prasad et al., 1984). Also, for oxidation of mixtures, it is usually assumed that each specie is oxidized independently (Prasad et al., 1984). (It is not implied here that the rate of oxidation of a specie in a mixture is identical to that as a single component.) Because all our experiments were carried out in large excesses of oxygen, a first-order kinetics assumption would enable us to determine a pseudo first-order rate constant for each oxidation reaction. With the further assumption of plug flow in the laboratory tubular reactor, a differential mass balance followed by integration yields the following equation for the pseudo first-order rate constant:

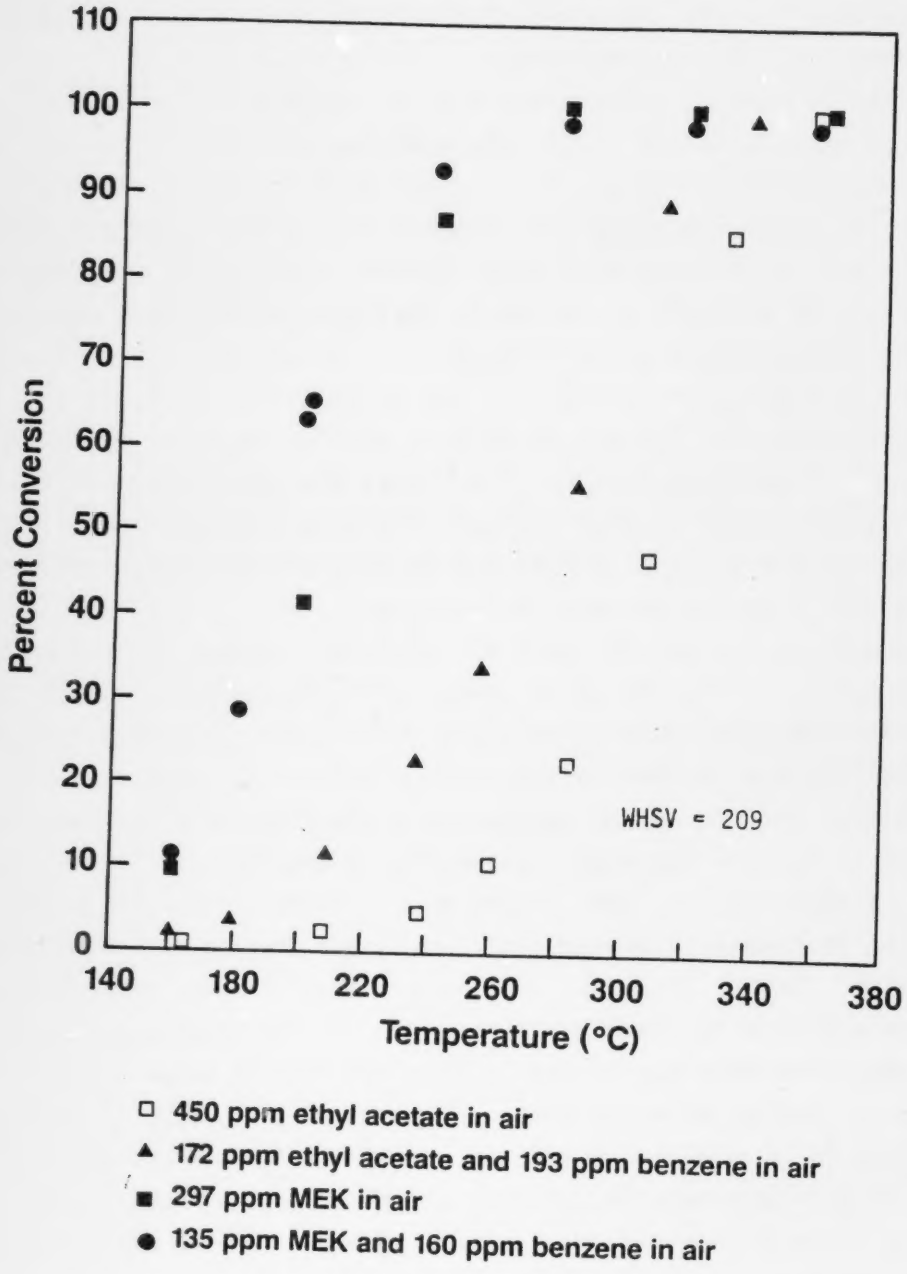

Figure 4-6. Comparison of the effect of benzene on ethyl acetate and MEK conversion.

$$k_{ps} = \frac{(WHSV)}{3600\ \rho_{GT}} \ln \frac{C_{io}}{C_i} \qquad (1)$$

where ρ_{GT} is the density of the gas (air) at temperature T.

k_{ps} may then be represented by the familiar Arrhenius equation

$$k_{ps} = A \exp [-E/RT] \quad . \qquad (2)$$

It is emphasized here that the above treatment should be regarded only as a way of representing the data because first-order kinetics may not apply. The advantages of the above equations are their simplicity and ability to represent a large amount of data concisely. It should also be noted that space velocity is incorporated into the first order equation so that data at different space velocities may be represented. A further advantage is that the Arrhenius plot may allow determination of temperature ranges for regions of surface-reaction control and mass-transfer control, as evident from Figure 4-7.

Figure 4-7 shows the first-order rate constants for the pure components. The order of reactivity of the four compounds is benzene ≃ MEK > n-hexane > ethyl acetate. The inlet concentrations of the gases for these data were 325, 297, 410, and 450 ppmv, respectively, for benzene, MEK, n-hexane, and ethyl acetate. The n-hexane plot exhibits apparent surface-reaction region below about 220°C. Also, linearity of the plot in the surface-reaction region suggests that first-order kinetics may be a reasonable approximation for n-hexane oxidation. The Arrhenius plot for benzene also shows apparent first-order behavior at low temperatures, but the plot for ethyl acetate shows a distinct curvature indicating that first-order kinetics may not be a reasonable representation. The plot for benzene also appears to show a shift into the mass-transfer region at a temperature just below 220°C, similar to the n-hexane plot.

Figure 4-7 for the single components is to be contrasted with the rate constants of the components in a ternary mixture (Figure 4-8). Ethyl acetate is now more reactive than n-hexane, and n-hexane's plot shows a curvature, indicating that first-order kinetics may not be obeyed in the mixture. Obviously, complex intercomponent interactions are present when mixtures are oxidized.

The apparent inhibitions and enhancements shown in Figures 4-2 through 4-6 may be caused by: (1) mixture effects involving competition for active

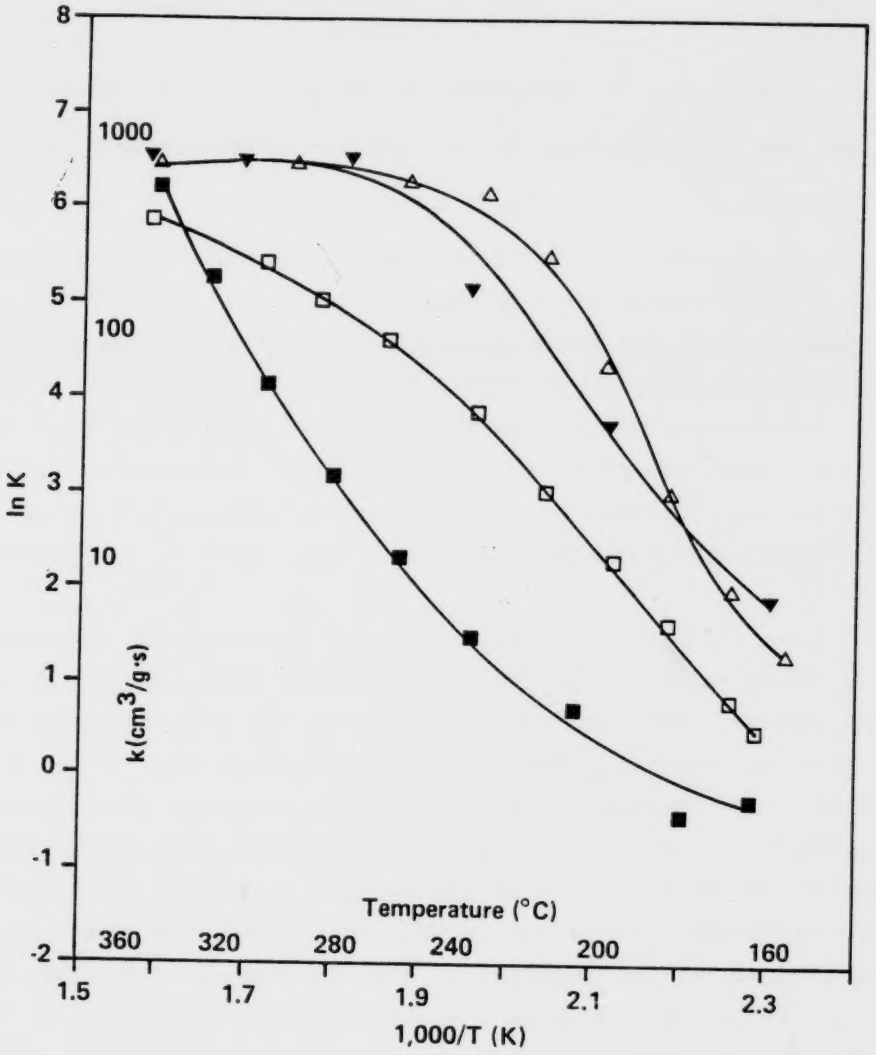

Figure 4-7. First order rate constants for the oxidation of single components.

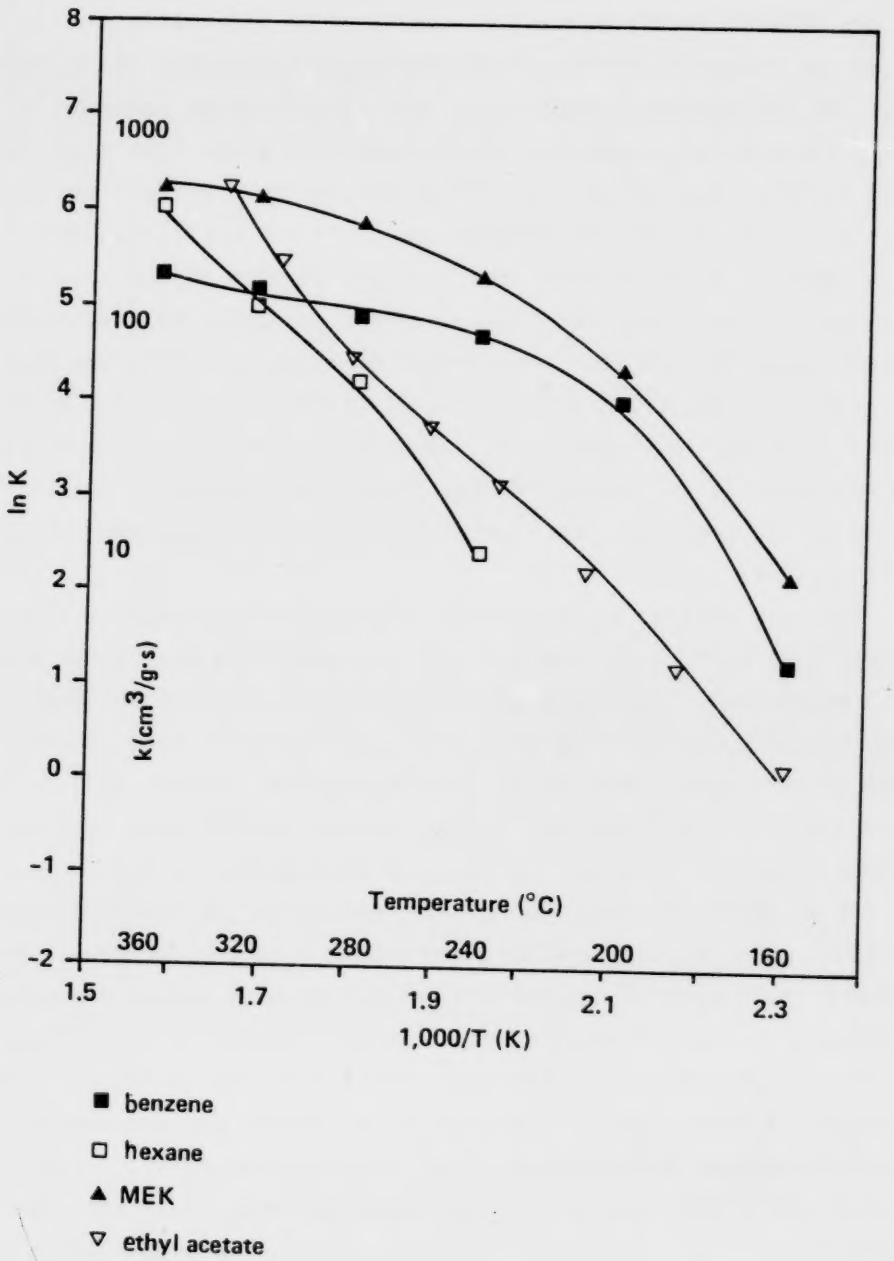

Figure 4-8. First order rate Constants for oxidation in a ternary mixture.

sites and differences in external and internal mass-transfer rates, and (2) mixture effects involving surface modification, cocatalysis or inhibition by one of the reacting species or intermediates (including the products CO_2 and H_2O). Of the reasons listed above, (1) appears to be mathematically tractable from surface kinetic data for single component given that a suitable kinetic model for the reaction of the various species in a mixture may be developed. Once this is done, and the effects are still not explained, then a combination of (1) and (2) above or some other unknown complex interactions are probably involved. To sort this out, it was deemed necessary to obtain intrinsic kinetic rates for the four components individually. This was done by operating the reactor as a differential reactor (conversions between 5 and 8 percent) for the four components individually at a series of concentrations and temperatures. The temperatures chosen were generally below 220°C (as guided by the previous experiments) to ensure that data were obtained in the surface kinetic region.

The rate data as a function of temperature and concentration are shown in Figures 4-9, 4-10, 4-11, and 4-12 for n-hexane, benzene, ethyl acetate, and MEK, respectively. n-Hexane exhibits close to first-order behavior at temperatures up to 201°C (Figure 4-9). On the other hand, benzene exhibits close to zero-order behavior at all temperatures tested, at concentrations above about 4×10^{-9} mol/cm^3. Ethyl acetate and MEK have reaction orders between 0 and 1. A power law fit gave an exponent of 0.7 in both cases. We may fit an empirical power law kinetic expression to the differential data for n-hexane, ethyl acetate and MEK, and assume a zero-order behavior for benzene. Although these kinetic expressions would represent single-component behavior accurately in the intrinsic kinetic region, they would not be useful for explaining the complex interactions observed in the catalytic oxidation of mixtures. A more rigorous approach is to develop kinetic expressions involving surface interactions (e.g., Langmuir/Hinshelwood, Eley/Rideal, or Mars/van Krevelen) because they may allow explanation of the complex interactions; e.g., via competitive adsorption. This approach has been adopted and is detailed in section 5.0 of this report.

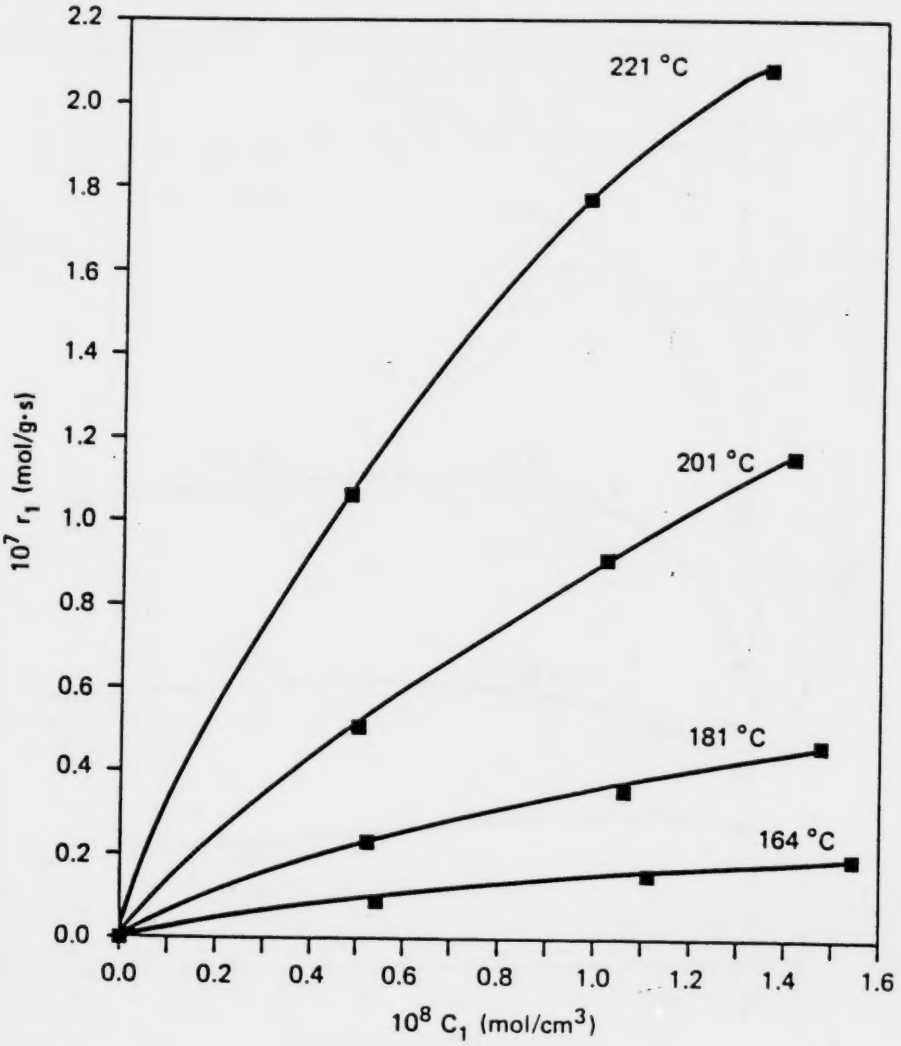

Figure 4-9. Differential reaction rate for n-hexane oxidation.

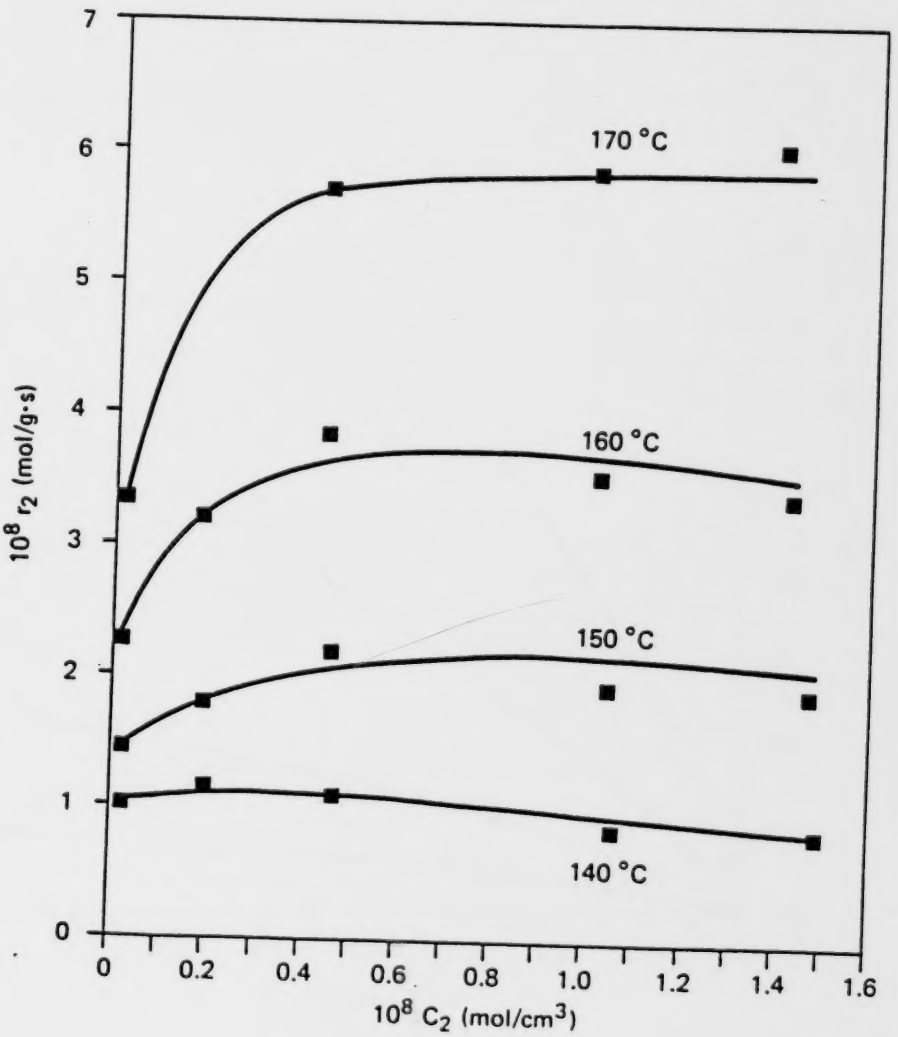

Figure 4-10. Differential reaction rate for benzene oxidation.

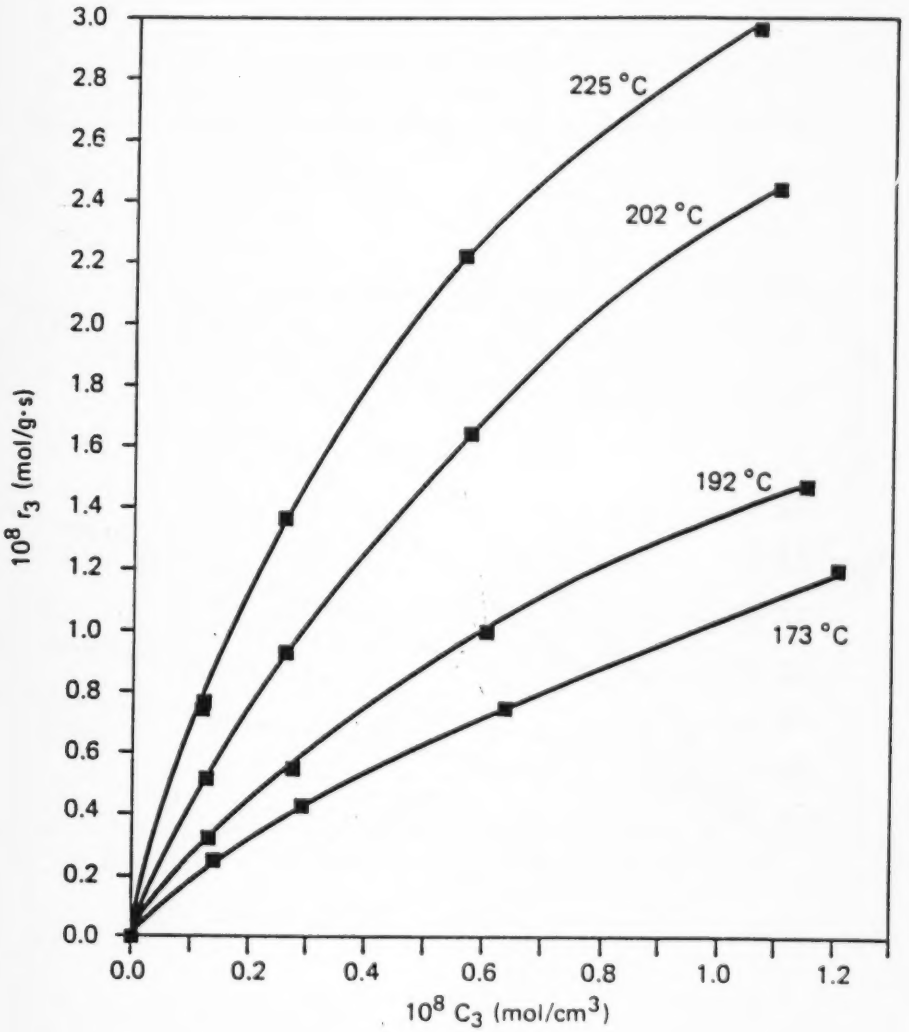

Figure 4-11. Differential reaction rate for ethyl acetate oxidation.

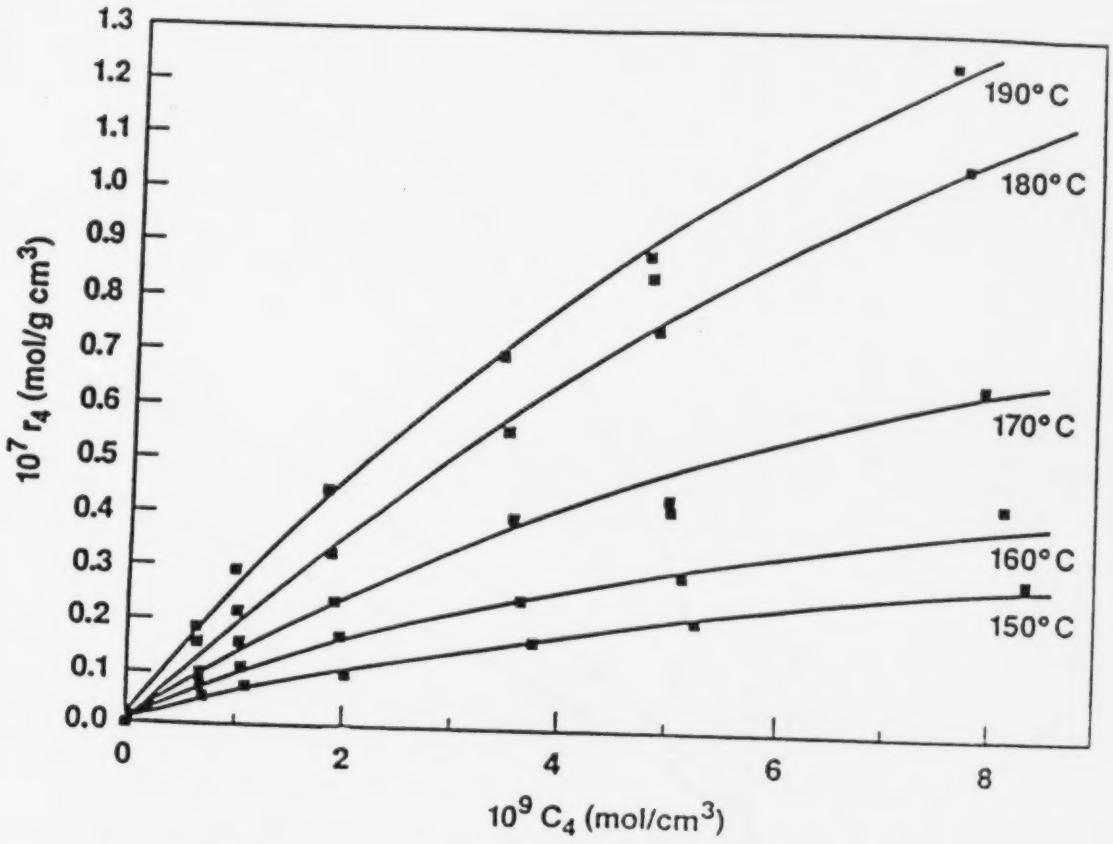

Figure 4-12. Differential reaction rate for MEK oxidation.

5.0 DEVELOPMENT OF A REACTOR MODEL FOR PREDICTING DEEP OXIDATION BEHAVIOR OF HYDROCARBON MIXTURES

As stated earlier, the conversions of n-hexane, benzene, ethyl acetate and MEK during isothermal oxidation were measured over a range of temperatures (Figures 4-2 to 4-5). These results show complex interactions as evident by the fact that single component conversions are different from those in mixtures for most of the hydrocarbon species studied. Mechanisms of possible interactions can be postulated in the form of mathematical kinetic models. The development of a multicomponent kinetic model is described below followed by its application to the specific reactor and catalyst configuration used in our experiments.

Development of Multi-Component Kinetic Model

The mechanistic kinetic model that has received the widest support (Balasubramanian and Vishwanath, 1975; Golodets, 1983; Jaswal et al., 1969) for oxidation of organic compounds is due to Mars and van Krevelen (1954) and is:

$$R_i + \text{oxidized catalyst} \xrightarrow{k_i} \text{reduced catalyst} + \text{products} \qquad (1)$$

$$O_2 + \text{reduced catalyst} \xrightarrow{k_{o_i}} \text{oxidized catalyst} \qquad (2)$$

In this mechanism, the above steps are assumed to be first order in the respective gaseous species. Thus, if Θ is the fraction of oxidized catalyst at any time, then:

$$r_i = k_i C_i \Theta \qquad (3)$$

and

$$r_{o_2} = k_{o_i} C_o (1-\Theta) \qquad (4)$$

If stoichiometry for oxidation requires γ_i moles of oxygen per mole of hydrocarbon, then:

$$r_{O_2} = \gamma_i r_i \tag{5}$$

from Equation (3), (4) and (5), eliminating θ,

$$r_i = \frac{k_{o_i} k_i C_o C_i}{k_{o_i} C_o + \gamma_i k_i C_i} \tag{6}$$

which is the Mars/van Krevelen rate expression for oxidation of hydrocarbon species i. Note that the apparent experimentally observed order of the hydrocarbon oxidation rate with respect to the hydrocarbon species varies between the extremes of 0 and 1. When:

$$k_{o_i} C_o \gg \gamma_i k_i C_i$$

then

$$r_i \cong k_i C_i \qquad \text{(first order with respect to hydrocarbon).} \tag{7}$$

and when $k_{o_i} C_o \ll \gamma_i k_i C_i$

$$r_i \cong \frac{k_o C_o}{\gamma_i} \qquad \text{(zero order with respect to hydrocarbon).} \tag{8}$$

The next step is to evaluate the respective k values for the components of interest, namely, n-hexane, benzene, ethyl acetate and MEK. This may be facilitated by inverting Equation (6):

$$\frac{1}{r_i} = \frac{1}{k_i} \cdot \frac{1}{C_i} + \frac{\gamma_i}{k_{o_i} C_o} \tag{9}$$

Because in our experiments C_o is nearly a constant due to the large excess of oxygen, Equation (9) should be a nearly linear relationship between inverse reaction rate and inverse concentration if Equation (6) adequately represents the oxidation rate data. Plots for $\frac{1}{r_i}$ vs. $\frac{1}{C_i}$ for n-hexane, ethyl acetate and MEK are shown in Figures 5-1, 5-2 and 5-3 respectively, for several

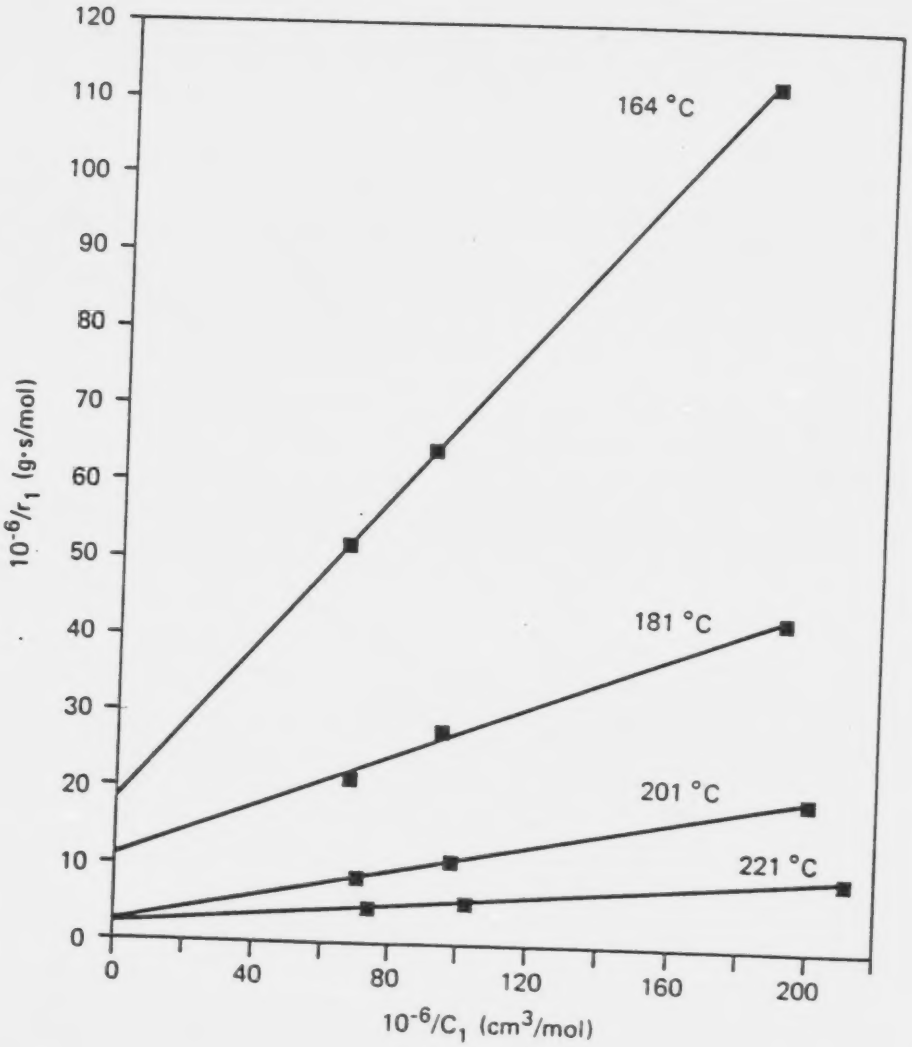

Figure 5-1. Inverse reaction rate versus inverse concentration for n-hexane oxidation.

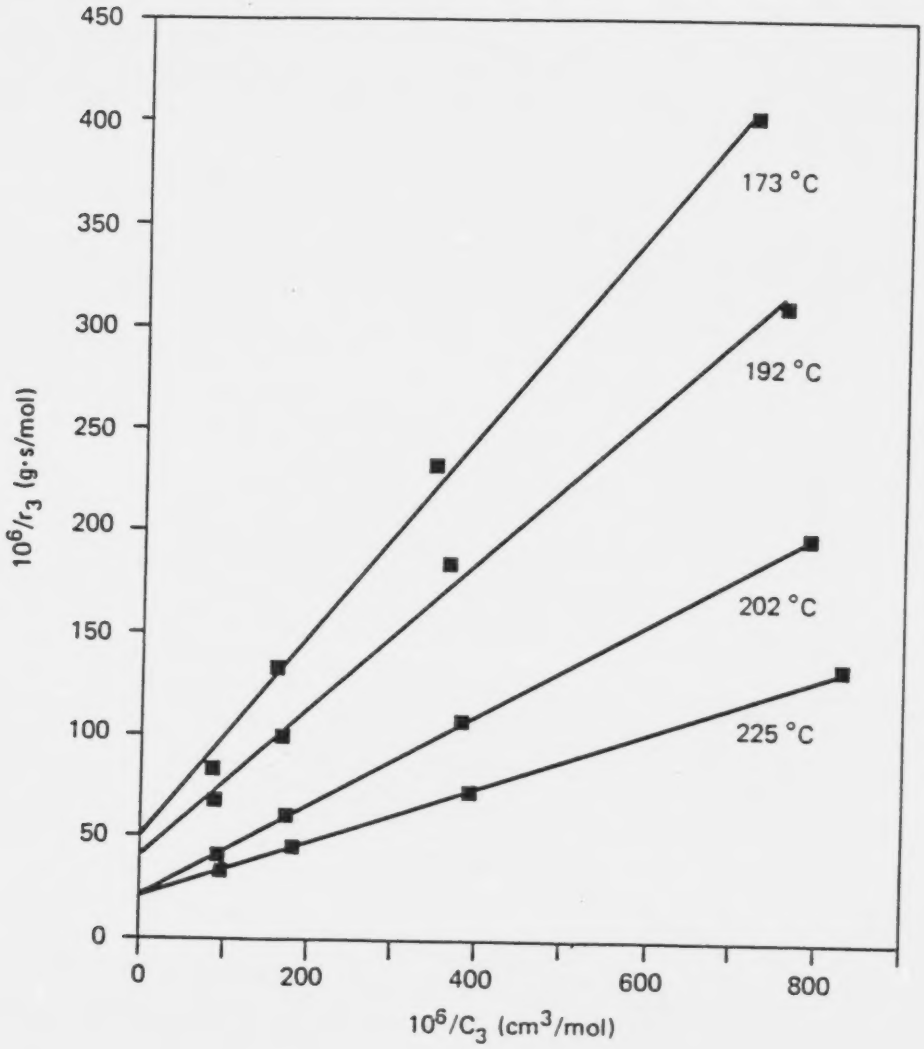

Figure 5-2. Inverse reaction rate versus inverse concentration for ethyl acetate oxidation.

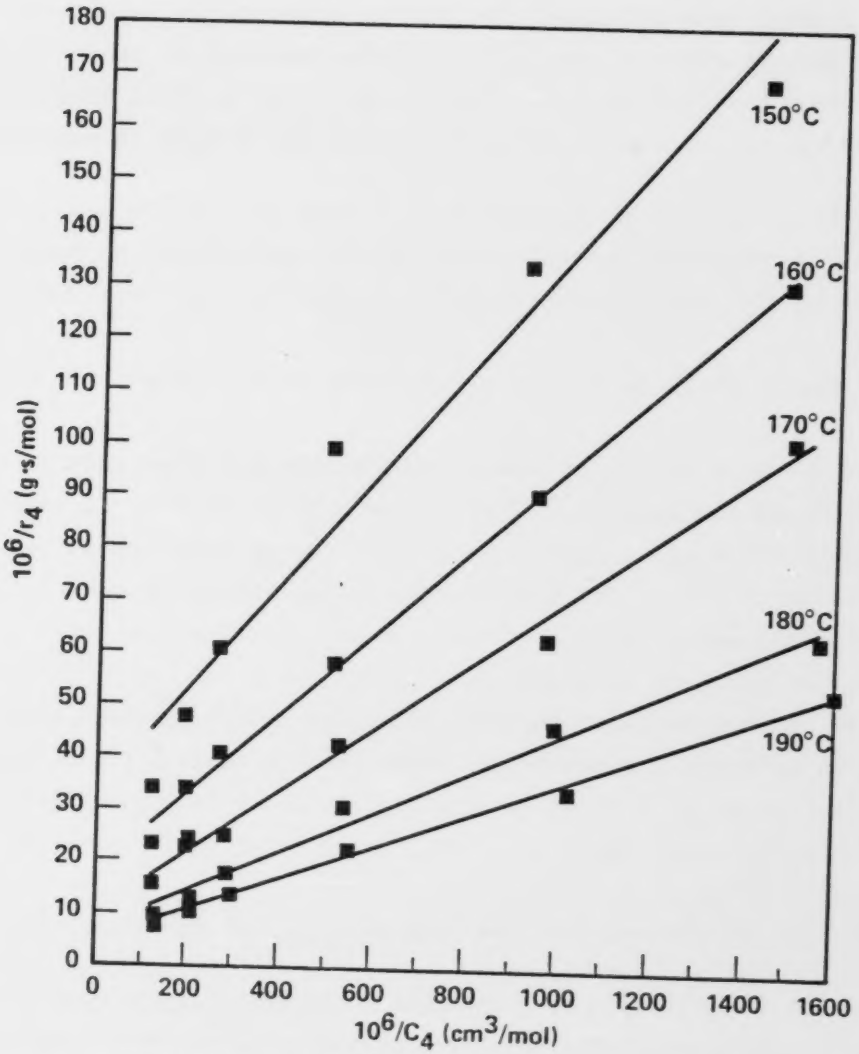

Figure 5-3. Inverse reaction rate versus inverse concentration for MEK oxidation.

temperatures. The linearity of these plots lends credence to the Mars/van Krevelen mechanism for these species. Arrhenius relationships and plots for the corresponding k values are shown in figures 5-4, 5-5 and 5-6.

A problem is encountered if a similar approach for benzene is attempted because benzene exhibits nearly a zero-order behavior at concentrations greater than $4 \cdot 10^{-9}$ mol/cm^3 (Figure 4-10). The limiting zero-order relationship is given by Equation (8), which may be used to evaluate k_{o_i} for benzene as a function of temperature from rate data in the nearly horizontal portions of the plots in Figure 4-10. k_i for benzene may be evaluated using the data at the lowest concentration from the limiting first-order Equation (7).

Arrhenius plots for k_i and k_{o_i} evaluated in this manner are shown in Figure 5-7. Only the three lowest temperatures have been used to evaluate k_i because it was not possible to obtain the data at the highest temperature under true differential reactor conditions due to experimental limitations. The behavior of MEK in the concentration range studied appears to fit equation (7) which represents the special case of Mars/van Krevelen kinetics where hydrocarbon oxidation controls.

The complete Mars/van Krevelen formulations for the four components for oxidation as single components are summarized in Table 5-1. To apply these relationships to the complex mixture effects shown in Figures 4-2 to 4-5, a multi-component model needs to be postulated based on the Mars/van Krevelen mechanism.

Because the reoxidation rate constants (k_{o_i}'s) for the various hydrocarbons are different, it is reasonable to assume that the catalytic specie is reduced to different oxidation states by the different hydrocarbons. n-Hexane, benzene, and ethyl acetate as R_1, R_2, and R_3, respectively, are designated. Then, for oxidation of a mixture of these hydrocarbons, the following may be postulated:

$$R_1 + \text{oxidized catalyst} \xrightarrow{k_1} [\text{reduced catalyst}]_1 + \text{products} \qquad (10)$$

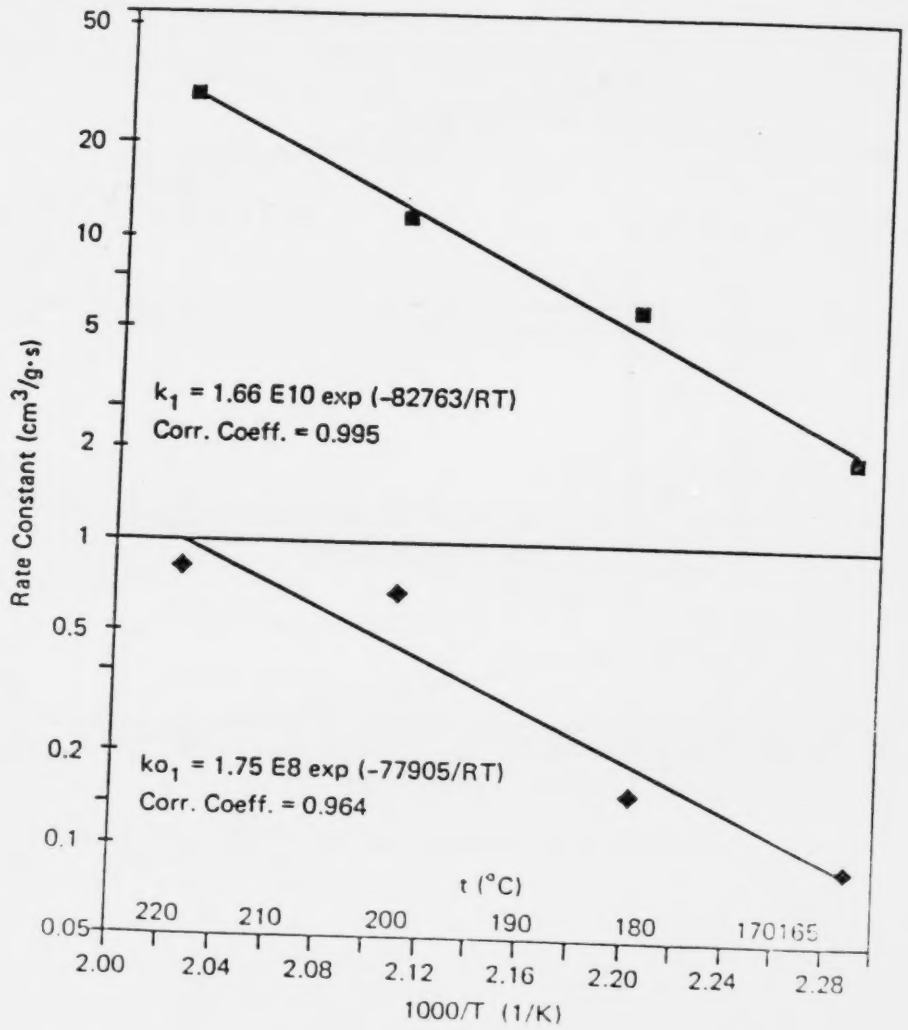

Figure 5-4. Mars/van Krevelen rate constants for n-hexane oxidation.

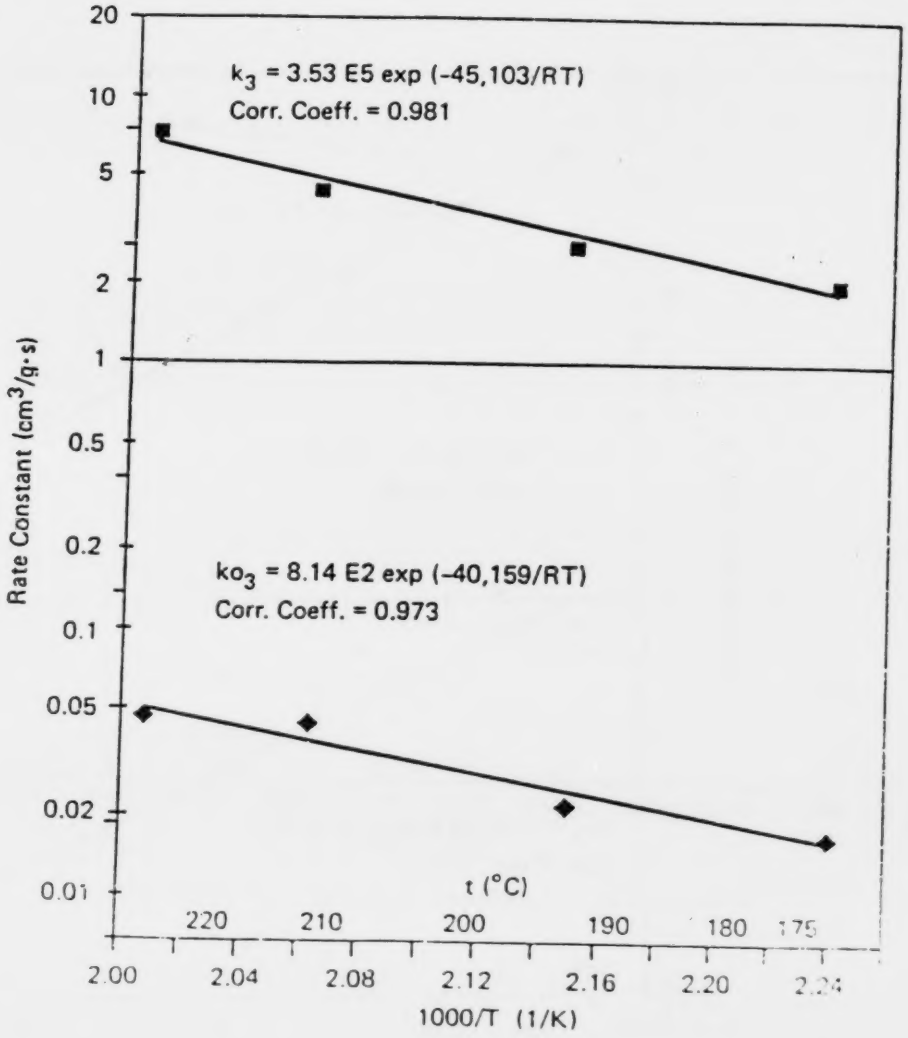

Figure 5-5. Mars/van Krevelen rate constants for ethyl acetate.

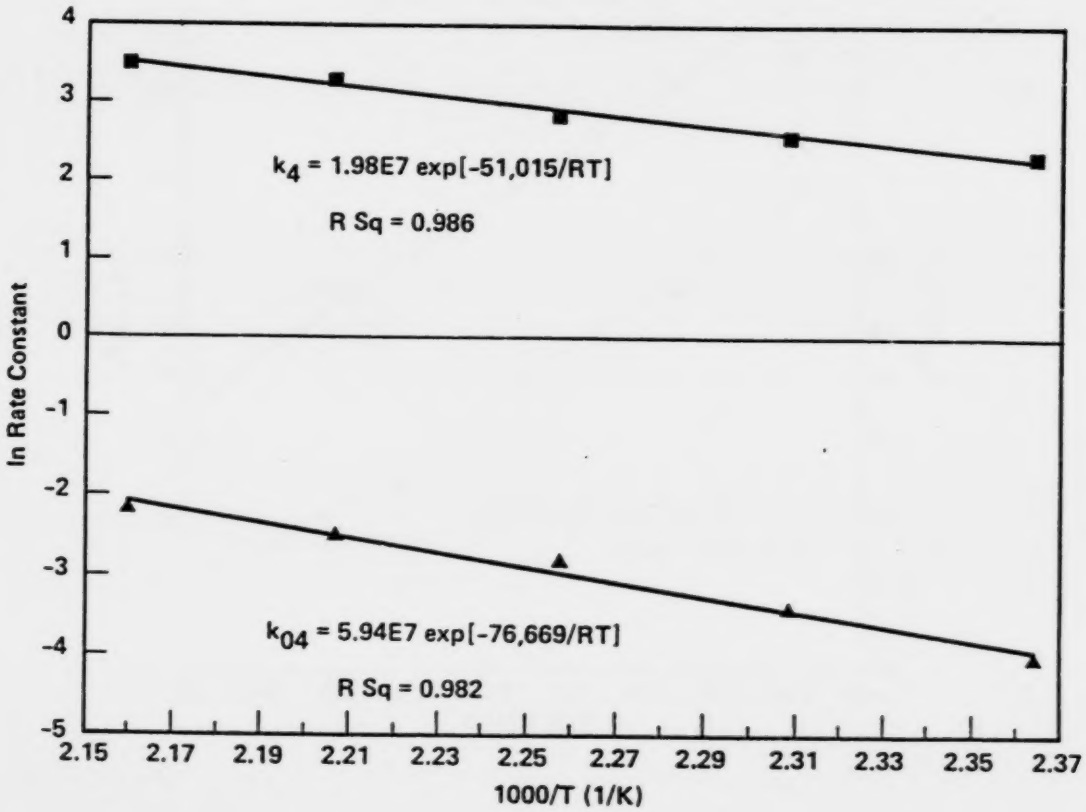

Figure 5-6. Mars/van Krevelen rate constants for MEK oxidation.

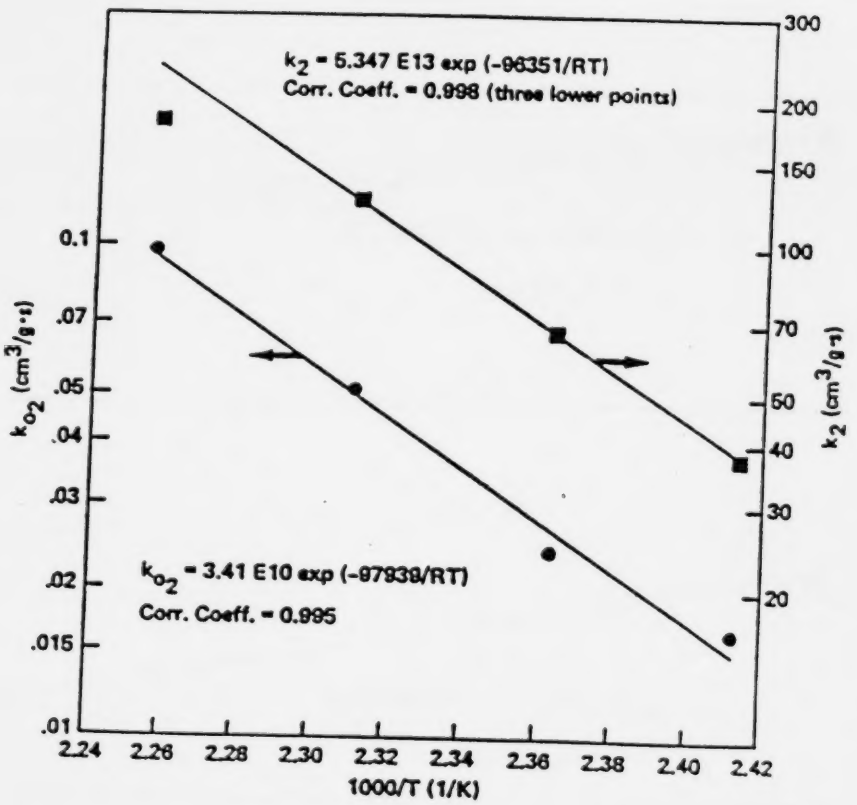

Figure 5-7. Mars/van Krevelen rate constants for benzene oxidation.

TABLE 5-1.

Mars/van Krevelen Rate Equation Parameters*

$$r_i = \frac{k_{oi}\, k_i\, C_o\, C_i}{k_{oi}\, C_o + \gamma_i\, k_i\, C_i}$$

	k_{oi}, $\frac{cm^3}{g \cdot s}$	k_i, $\frac{cm^3}{g \cdot s}$	γ_i (–)
n-hexane	$1.75 \cdot 10^{8} \exp[-77{,}905/RT]$	$1.660 \cdot 10^{10} \exp[-82{,}763/RT]$	9.5
benzene	$3.41 \cdot 10^{10} \exp[-97{,}939/RT]$	$5.347 \cdot 10^{13} \exp[-96{,}351/RT]$	7.5
ethyl acetate	$8.14 \cdot 10^{2} \exp[-40{,}159/RT]$	$3.533 \cdot 10^{4} \exp[-45{,}108/RT]$	5.0
MEK	$5.94 \cdot 10^{7} \exp[-76{,}669/RT]$	$1.98 \cdot 10^{7} \exp[-51{,}015/RT]$	5.5

*$R = 8.314\ J\ mol^{-1}\ K^{-1}$

$$O_2 + [\text{reduced catalyst}]_1 \xrightarrow{k_{o_1}} \text{oxidized catalyst} \qquad (11)$$

$$R_2 + \text{oxidized catalyst} \xrightarrow{k_2} [\text{reduced catalyst}]_2 + \text{products} \qquad (12)$$

$$O_2 + [\text{reduced catalyst}]_2 \xrightarrow{k_{o_2}} \text{oxidized catalyst} \qquad (13)$$

$$R_3 + \text{oxidized catalyst} \xrightarrow{k_3} [\text{reduced catalyst}]_3 + \text{products} \qquad (14)$$

$$O_2 + [\text{reduced catalyst}]_3 \xrightarrow{k_{o_3}} \text{oxidized catalyst} \qquad (15)$$

If at any instant θ_1, θ_2, θ_3 are the fractions of the catalyst surface occupied by $[\text{reduced catalyst}]_1$, $[\text{reduced catalyst}]_2$, and $[\text{reduced catalyst}]_3$, respectively, then the following balances may be written:

$$r_1 = k_1 C_1 (1-\theta_1 -\theta_2 -\theta_3) = \nu_1 k_{o_1} C_o \theta_1 \qquad (16)$$

$$r_2 = k_2 C_2 (1-\theta_1 -\theta_2 -\theta_3) = \nu_2 k_{o_2} C_o \theta_2 \qquad (17)$$

$$r_3 = k_3 C_3 (1-\theta_1 -\theta_2 -\theta_3) = \nu_3 k_{o_3} C_o \theta_3 \qquad (18)$$

θ_1, θ_2, and θ_3 may be evaluated from Equations (16), (17), and (18) and substituted in the right-hand sides of these equations to yield the respective rate equations for oxidation in a mulicomponent mixture:

$$r_1 = \frac{k_{o_1} k_i C_o C_1}{k_{o_1} C_o + \nu_1 k_1 C_1 + \nu_2 \frac{k_{o_1}}{k_{o_2}} k_2 C_2 + \nu_3 \frac{k_{o_1}}{k_{o_3}} k_3 C_3} \qquad (19)$$

$$r_2 = \frac{k_{o_2} k_2 C_o C_2}{k_{o_2} C_o + \nu_2 k_2 C_2 + \nu_1 \frac{k_{o_2}}{k_{o_1}} k_1 C_1 + \nu_3 \frac{k_{o_2}}{k_{o_3}} k_3 C_3} \qquad (20)$$

$$r_3 = \frac{k_{o_3} k_3 C_o C_3}{k_{o_3} C_o + \gamma_3 k_3 C_3 + \gamma_1 \frac{k_{o_3}}{k_{o_1}} k_1 C_1 + \gamma_2 \frac{k_{o_3}}{k_{o_2}} k_2 C_2} \qquad (21)$$

A general rate from for deep oxidation of the ith component in an n-component mixture may be easily inferred from Equations (19) to (21):

$$r_i = \frac{k_{o_i} k_i C_o C_i}{k_{o_i} C_o + \sum_{j=1}^{n} \frac{k_{o_i}}{k_{o_j}} \gamma_j k_j C_j} \quad , \quad i = 1,2,\ldots \quad . \qquad (22)$$

Development of Reactor Model

In this section, we describe the application of the multicomponent intrinsic kinetic rate expression (Equation 22) to the specific reactor and catalyst used in our experiments. The ultimate objective is to develop a reactor model which would predict the complex behavior observed in Figures 4-2 through 4-5.

Since a tubular reactor is used, at high conversions typical of higher temperatures in Figures 4-2 to 4-5, the concentration of the hydrocarbon species changes considerably along the catalytic reactor bed. Thus the kinetic rate of reaction changes along the bed and a differential equation is needed to describe the reactor concentration profile as a function of catalyst bed depth (or catalyst weight). Additional complication is caused by the possibility of diffusional limitations into the catalyst porous structure at high temperatures. Typically this would result in a global rate of reaction which is slower than the kinetic rate and must be accounted for in the reactor model. Thus, at any depth along the reactor bed, a concentration profile will exist within the catalyst particles themselves and this will give rise to a particle differential equation for concentration within the particle as a function of particle radius. The reactor differential equation and the particle differential equation will be coupled through a concentration boundary condition at the external surface of the catalyst particle.

Two types of boundary conditions may be considered. It may be assumed that the mass transfer across the gas film around the particle is equal to the diffusive flux into the particle:

$$-D_{eff(i)} \left(\frac{dC_{ik}}{dR}\right)\Big|_{R_o} = k_{f(i)} (C_i - C_{ik}) \Big|_{R_o} \qquad (23)$$

or the external mass transfer resistance may be neglected:

$$C_i \Big|_{R_o} = C_{ik} \Big|_{R_o} \qquad (24)$$

In the model development described below, the external mass transfer resistance has been neglected because it is expected to hinder the rate of reaction to a lesser extent than the internal diffusion (pore diffusion) resistance. The reactor model equations for an n-component hydrocarbon mixture is presented in Table 5-2. These equations have been obtained by the mole balance of species i for a differential section along the bed (reactor equations) and for a differential section within the catalyst particle (particle equations).

Numerical methods are required to solve the coupled differential equations in Table 5-2. To facilitate the solution, the equations were non-dimensionalized. These non-dimensionalized equations are presented in Table 5-3.

Before presenting the solution methods used, it is instructive to consider the simpler case of the reactor model where internal diffusional resistances are neglected. In this special case, the particle equation is not considered and the reaction equation reduces to:

$$\frac{dC_i}{dw} = \frac{(-r_i)}{v} \quad , \quad (i = 1,2,3\ldots) \qquad (35)$$

with inlet condition $C_i\ (0) = C_{io}$, $(i = 1,2,3\ldots)$ (36)

In dimensionless form Equations (35) and (36) may be written as:

$$\frac{d\alpha_i}{dw} = \beta \frac{\alpha i}{1 + \sum_{i=1}^{n} k_i \alpha_i} \quad , \quad (i = 1,2,3\ldots) \tag{37}$$

$$\alpha_i\ (0) = 1 \quad , \quad (i = 1,2,3\ldots) \tag{38}$$

The fractional conversion of the ith species is defined as:

$$f_i = 1 - \frac{C_i}{C_{io}} = 1 - \alpha_i \tag{39}$$

Equations (37) and (38) were solved by a fourth-order Runge-Kutta method to obtain the fractional conversion in mixtures at the bed exit for a series of temperatures. Only the results for the binary mixtures of n-hexane and benzene, and n-hexane and ethyl acetate are presented because similar results were obtained for other mixtures. The model evaluations for the two binary mixtures (n-hexane/benzene and n-hexane/ethyl acetate) are compared to the actual experimental results (from Figures 4-2 through 4-4) in Figures 5-8 and 5-9, respectively.

Considering Figure 5-8 first, the model overpredicts somewhat the experimentally observed conversions of benzene throughout the temperature range and is adequate for n-hexane up to approximately 220°C. Above 220°C the model begins to overpredict the experimentally observed conversions for both components. The overprediction of n-hexane begins to rapidly increase at the point where benzene is nearly completely consumed as predicted by the model. The reason for this is that the magnitude of the denominator (adsorption term) of Equation (22) strongly affects the rate for either component and is a function not only of the rate constants but also of the concentrations. Since benzene is overpredicted in the kinetic region, the magnitude of the adsorption term for benzene is overpredicted in the kinetic region, the magnitude of the adsorption term for benzene must be actually somewhat greater than that given by the proposed multicomponent Mars/van Krevelen model. A more rigorous model is thus needed which results in a larger adsorption term for benzene. One possibility is the strong chemisorption of reaction products

TABLE 5-2. MULTICOMPONENT OXIDATION MODEL WITH INTERNAL DIFFUSION

Reaction Equations $(i = 1,2,3....)$

$$\frac{dC_i}{dW} = \frac{3D_{eff(i)}}{vR_o\rho_p}\left[\frac{dC_{ik}}{dR}\right]_{R_o} \tag{25}$$

Inlet conditions: $C_i\ (0) = C_{i_o}$ (26)

Particle Equations $(i = 1,2,3...)$

$$\frac{d^2C_{ik}}{dR^2} + \frac{2}{R}\frac{dC_{ik}}{dR} = \frac{(-r_{ik})\ \rho_p}{D_{eff(i)}} \tag{27}$$

Boundary conditions:

$$C_{ik}\Big|_{R_o} = C_i\Big|_{R_o} \tag{28}$$

$$\frac{dC_{ik}}{dR}\Big|_0 = 0 \tag{29}$$

where r_{ik} is given by equation (22). the subscript i represents the hydrocarbon species. and the subscript k represents conditions within the particle.

The assumptions made in the development of Table 5-2 equations are:

(1) the tubular reactor flow hydrodynamics may be approximated by plug-flow behavior

(2) the external mass transfer resistance is negligible

(3) the particles are spherical with center symmetry

(4) the reactor is isothermal and the change in volumetric flow rate (v) due to reaction is negligible.

TABLE 5-3. MULTICOMPONENT OXIDATION MODEL IN NON-DIMENSIONAL FORM

Reactor Equations ($i = 1,2,3\ldots$)

$$\frac{d\alpha_i}{dw} = \lambda_i \left.\frac{d\alpha_{ik}}{d\eta}\right|_1 \tag{30}$$

Inlet conditions: $\alpha_i\,(0) = 1$ (31)

Particle Equations ($i = 1,2,3\ldots$)

$$\frac{d^2\alpha_{ik}}{d\eta^2} + \frac{2}{\eta}\frac{d\alpha_{ik}}{d\eta} = h_i{}^2 \left[\frac{\alpha_{ik}}{1 + \sum_{i=1}^{n} k_i\alpha_{ik}}\right] \tag{32}$$

Boundary Conditions:

$$\alpha_{ik}\Big|_1 = \alpha_i \tag{33}$$

$$\left.\frac{d\alpha_{ik}}{d\eta}\right|_0 = 0 \tag{34}$$

(e.g. water) which would increase the magnitude of the adsorption term. This will reduce benzene conversion and thereby correctly predict n-hexane conversion as well at the higher temperatures. At the higher temperatures, the increase in overprediction may also be caused due to diffusional effects.

More severe limitation of the model is seen in Figure 5-9. The model overpredicts n-hexane conversion nearly throughout the temperature range and underpredicts ethyl acetate beyond about 210°C. The overprediction of n-hexane in Figure 5-9 at temperatures below 220°C indicates complex effects in the intrinsic kinetic region, associated with the presence of an oxygenated specie (i.e., ethyl acetate) as opposed to a nonoxygenated specie (i.e., benzene in Figure 5-8).

Predictions using the proposed model for other mixtures containing ethyl acetate are not shown herein but were similar. For example, for benzene/ethyl acetate mixture, the model overpredicted benzene conversion and severely underpredicted ethyl acetate conversion past the temperature of about 210°C. For the ternary benzene/ethyl-acetate/n-hexane mixture, the model over-predicted the conversions of benzene and n-hexane and underpredicted the conversion of ethyl acetate past the temperature of 210°C.

The breakdown of the model in the presence of ethyl acetate suggests that the partially oxygenated structure of ethyl acetate may play a strong role in multicomponent oxidation kinetics. A more rigorous multicomponent kinetic model is needed. It is impossible that reaction products such as water may hinder the oxidation of non-oxygenated species but enhance the oxidation of oxygenated species via alternative reactions such as hydrolysis. This may account for the underprediction of ethyl acetate between 210 and 220°C and the overprediction of n-hexane. Beyond 220°C however, the underprediction of ethyl acetate is quite severe and suggests the advent of simultaneous gas phase reactions with higher activation energies. This is discussed further after the modeling results of the pore diffusion model are presented.

We next consider the case where the inhibiting effect of internal diffusion (pore diffusion) on the rate has been taken into account by

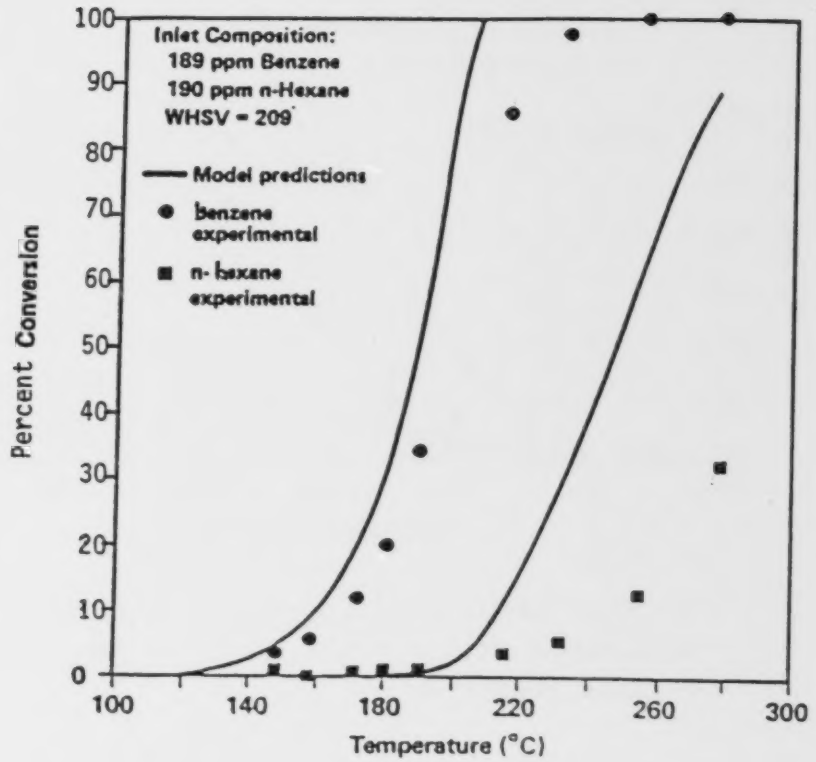

Figure 5-8. Comparison of predicted and actual conversions for benzene and n-hexane in a binary mixture.

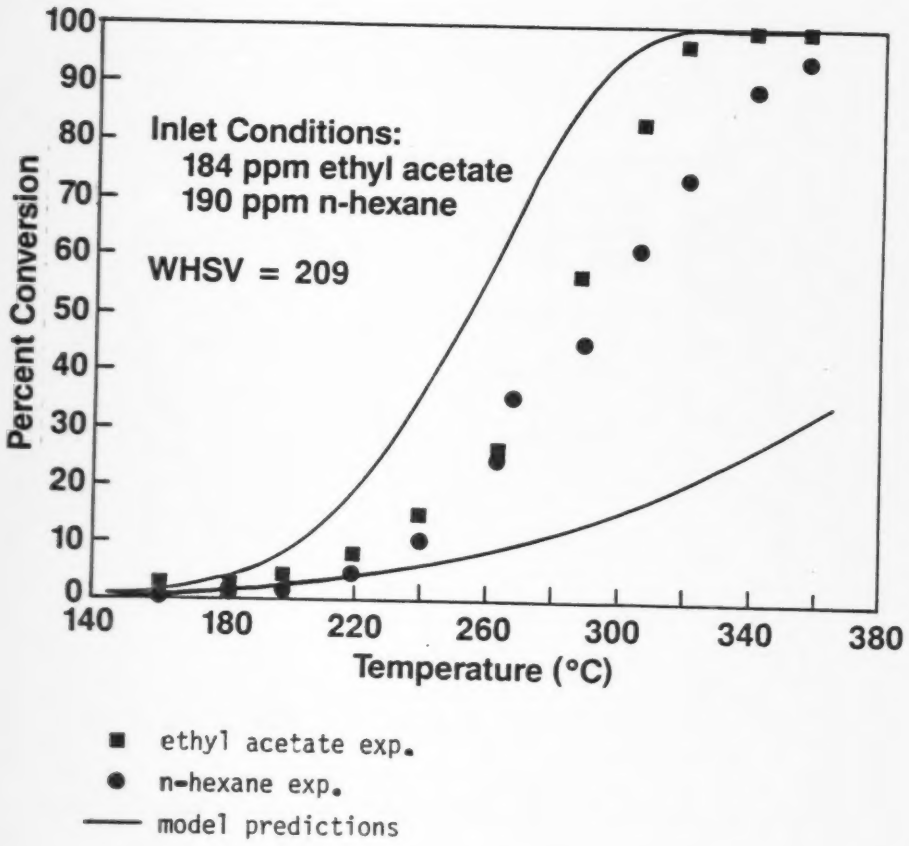

Figure 5-9. Comparison of predicted and actual conversions for ethyl acetate and n-hexane in a binary mixture.

considering the reactor equation and particle equation separately (Tables 5-2 and 5-3).

The particle equations in Table 5-3 were solved by first converting the second order particle differential equation into two first order differential equations. Equations (32) through (34) were rewritten as:

$$\frac{d\alpha_{ik}}{dn} = m_i \quad . \ (i = 1,2,3\ldots) \tag{40}$$

$$\frac{dm_i}{dn} + \frac{2m_i}{n} = h_i^2 \left[\frac{\alpha_{ik}}{1 + \sum_{i=1}^{n} k_i \alpha_{ik}} \right] \quad . \ (i=1,2,3\ldots) \tag{41}$$

With boundary conditions:

$$\alpha_{ik}\Big|_1 = \alpha_i \ , \quad (i = 1,2,3\ldots) \tag{42}$$

and $$m_i\Big|_0 = 0 \quad . \ (i = 1,2,3\ldots) \tag{43}$$

The problem is now to solve Equations (31), (32) and (40) through (43) simultaneously using a numerical technique. The primary difficulty in using a straight forward Runge-Kutta method is that the concentration at the center of the particle is unknown, thus an initial condition required to advance the Runge-Kutta iteration is not available.

Our approach around this difficulty involved a trial and error solution. Before presenting the method of solution, however, it is necessary to estimate the effective diffusivity, $D_{eff(i)}$ for each hydrocarbon species. This parameter is a function of both the hydrocarbon type and the complex porous structure of the catalyst. The catalyst used (G-43, United Catalyst, Inc.) has a bimodal pore distribution as shown in Table 5-4.

TABLE 5-4. CATALYST PHYSICAL PROPERTIES FOR MODELING AND $D_{eff(i)}$ CALCULATION

Pore Size Range (nm)	Pore Volume Contained (cm^3/g)
1.4 - 2.9	0.03
2.9 - 14	0.24
14 - 80	0.00
80 -150	0.08
Total Pore Volume =	0.35 cm^3/g

Particle Density, ρ_p = 1.46 g/cm^3
Surface Area, S_g = 212 m^2/g
Micropore Void Fraction, ε_m = 0.394
Macropore Void Fraction, ε_u = 0.117
Average Micropore Radius, $_u$ = 2.57 nm
Average Macropore Radius, $_u$ = 57.5 nm

The random pore model proposed by Wakao and Smith, (1962) was used to estimate $D_{eff(i)}$ for each hydrocarbon species. This model is given by

$$D_{eff(i)} = \bar{D}_{Mi}\ \varepsilon_M^2 + \frac{\varepsilon_u^2\ (1 + 3\ \varepsilon_M)}{1 - \varepsilon_M}\ \bar{D}_{ui} \qquad (44)$$

where $$\frac{1}{D_{Mi}} = \frac{1}{D_{i\text{-}air}} + \frac{1}{(D_K)_{Mi}} \qquad (45)$$

and $$\frac{1}{D_{ui}} = \frac{1}{D_{i\text{-}air}} + \frac{1}{(D_K)_{ui}} \qquad (46)$$

$D_{i\text{-}air}$ for each hydrocarbon species was estimated from the Chapman-Enskog formula:

$$D_{i\text{-}air} = \frac{.0018583\ T^{3/2}\ \left[\frac{1}{(MW)_i} + \frac{1}{(MW)_{air}}\right]^{1/2}}{P\sigma_{i\text{-}air}\ \Omega_{i\text{-}air}} \tag{47}$$

$$\text{where} \quad \sigma_{i\text{-}air} = \frac{1}{2}\left[\sigma_i + \sigma_{air}\right] \tag{48}$$

$$\text{and} \quad \Omega_{i\text{-}air} = \text{function of } \frac{K_B T}{\varepsilon_{i\text{-}air}} \tag{49}$$

$$\text{and} \quad \varepsilon_{i\text{-}air} = (\varepsilon_i\ \varepsilon_{air})^{1/2} \tag{50}$$

The σ and ε values are directly available for the hydrocarbon species of interest and air in standard kinetics texts (Smith,1981). The collision integral $\Omega_{i\text{-}air}$ is a function of $\frac{K_B T}{\varepsilon_{i\text{-}air}}$. For the temperature range of interest, this value was estimated by the following equation (obtained by curve fitting) to facilitate substitution into the numerical method:

$$\Omega_{i\text{-}air} = .713\ \log_{10}\left[\frac{K_B T}{\varepsilon_{i\text{-}air}}\right] + 1.2874 \tag{51}$$

The fit of the above equation with actual published values is shown in Figure 5-10.

$(\bar{D}_K)_{Mi}$ and $(\bar{D}_K)_{ui}$, the respective Knudsen diffusion coefficients in the macro- and micro-pore regions were calculated from

$$D_K = 9.7 \times 10^3 \bar{r} \left(\frac{T}{(MW)_i} \right)^{1/2} \tag{52}$$

where $\bar{r}$ is the average pore radius (Table 5-4). Thus knowing $\bar{D}_{Mi}$ and $\bar{D}_{ui}$ from Equations (47) and (48) and ε_M and ε_u (from Table 5-4), $D_{eff(i)}$ was calculated for each hydrocarbon species as a function of temperature.

Once D_{eff} was known, all parameters in Table 5-3 model equations are available. The method of solution involved first dividing the catalyst bed into a number of grids.

At the first grid (i.e., at the entrance to the bed) the particle equations were then solved. The solution was carried out by a combination of the sixth order Runge-Kutta-Verner method (IMSL Routine DVERK) and a global constrained function minimizer (IMSL subroutine ZXMWD) on an IMB 370 mainframe computer. A guess value is assigned at the particle center for each hydrocarbon species concentration. The Runge-Kutta is solved and the concentration at the external surface is compared to bed inlet concentration. The difference is minimized (by minimizing the sum of the square of the dimensionless concentration differences of the various species) until it is close to 0. The radial gradient at the surface is then evaluated and substituted in Equation (30) to advance the bed dimensionless concentration to the next grid. The above operations are repeated until the concentration profile in the bed is completely determined. The accuracy of the solution can be increased by increasing the number of grids. We have found 20 grids to be a reasonable number in our solution.

Comparisons of model predictions to experimental data are presented in Figures 5-11 to 5-14. The predictions in Figures 5-11 through 5-13 are shown with and without pore diffusion incorporated into the model. The negligible difference in the predictions demonstrate the absence of pore diffusion

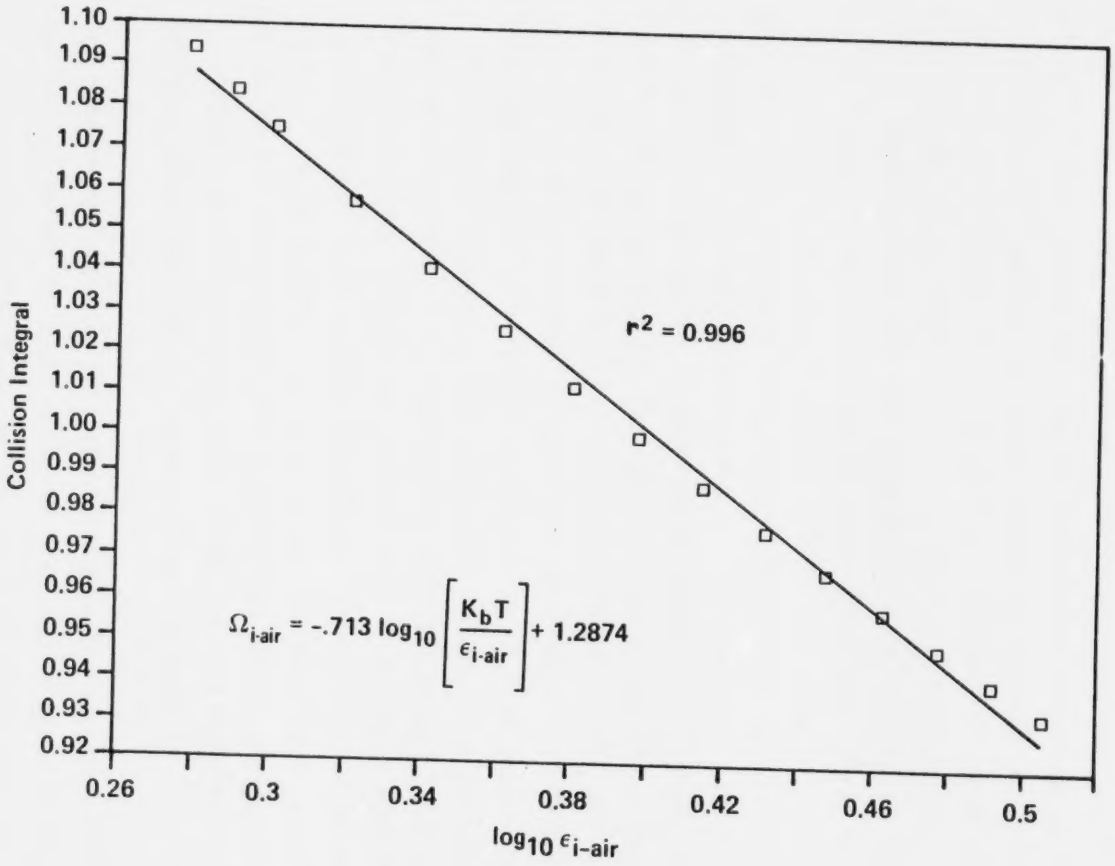

Figure 5-10. Evaluation of collision integral for modeling purposes in the temperature range of interest.

inhibitions for the 120-170 mesh particles used in our experiments. The pore diffusion model, however, is quite useful for larger particles (e.g. 6 mm) typical of industrial reactors. From Figure 5-11, both models over-predict simple component n-hexane data above about 260°C indicating that external diffusion effects may become significant above 260°C. A second possibility is the retardation of the kinetics by reaction products such as water which would be more apparent at higher conversions as obtained above 260°C. From Figure 5-12, the effect of external diffusion is not so apparent for benzene. The pore diffusion model is somewhat superior at higher conversions than the simpler model without internal diffusion. From Figure 5-13, the benzene data in the mixture is overpredicted throughout the temperature range, confirming the need for a larger adsorption term for benzene in the kinetic equation (as concluded previously using the simpler model). Also, as stated previously, the presence of strong water chemisorption will lead to a bigger adsorption term and may allow a superior fit. Experiments at varying inlet humidities are needed to verify this. Once the benzene is correctly predicted, n-hexane would be better predicted as well because the overprediction of n-hexane conversion in the mixture beyond about 210°C is believed to be due to a smaller adsorption term resulting from benzene overprediction.

Finally, Figure 5-14 shows the comparison of single component ethyl acetate conversion predicted by the simple model to experimental data. The fit in the kinetic region (>220°C) is excellent, indicating the suitability of Mars/van Krevelen kinetics in this region. At >220°C, the conversions increase much more rapidly with temperature indicating a significantly higher activation energy than given by the Mars/van Krevelen kinetics. The increased activation energy may be due to the onset of catalytically supported thermal reactions and differential data needs to be collected in this higher temperature region to develop a better model to represent ethyl acetate oxidation.

Summarizing the modeling work to date, a simple multicomponent kinetic model based on the single component Mars/van Krevelen mechanism was found to be adequate for predicting oxidation of non-oxygenated hydrocarbon such as benzene and n-hexane. At the trace level concentrations used, however, water formed from reaction may inhibit the kinetics. The pore diffusion model

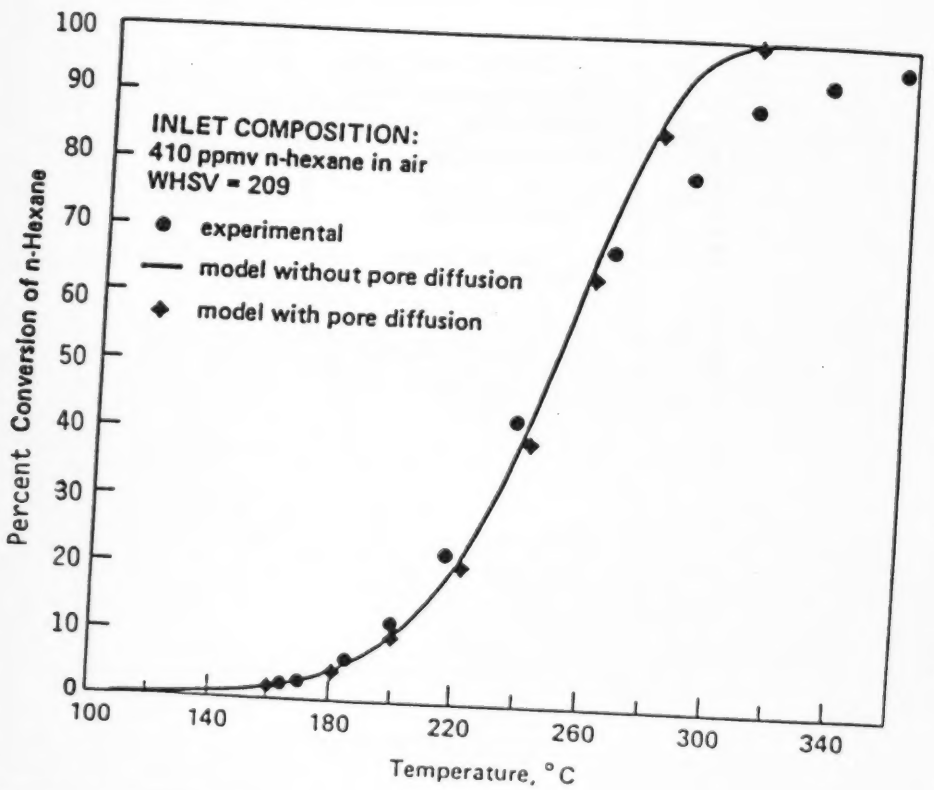

Figure 5-11. Comparison of model predictions and experimental data for n-hexane conversion as a single component.

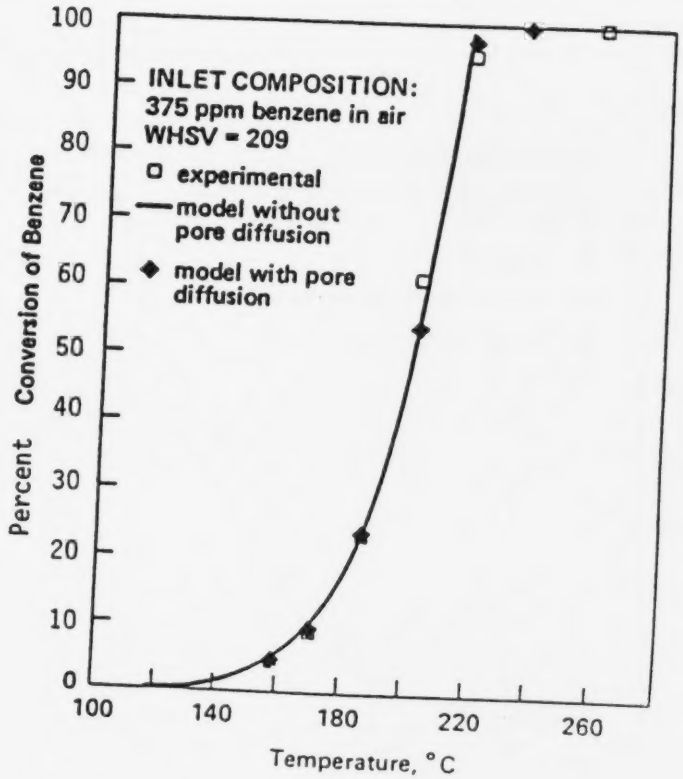

Figure 5-12. Comparison of model predictions and experimental data for benzene conversion as a single component.

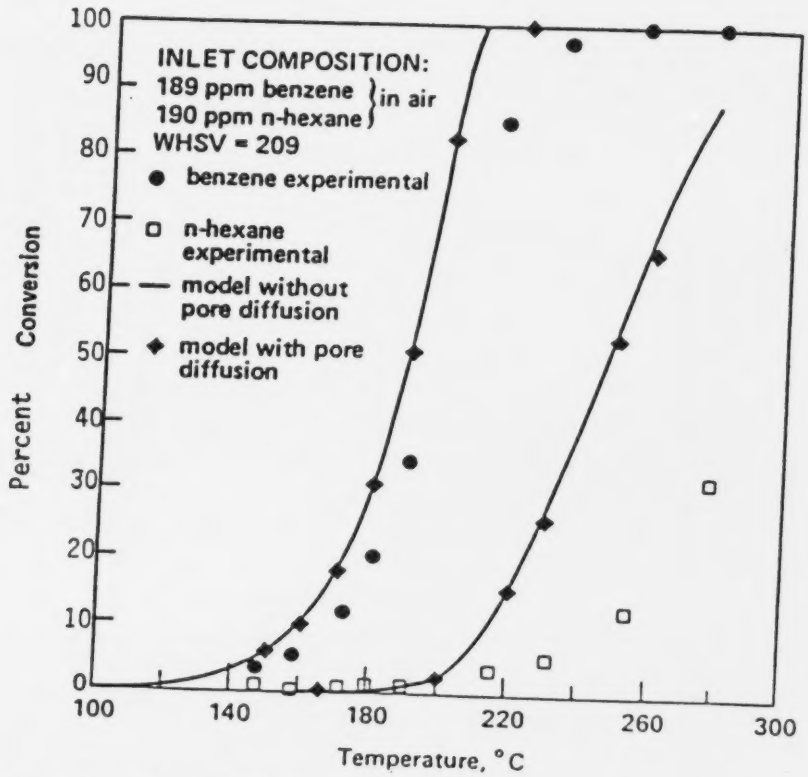

Figure 5-13. Comparison of model predictions and experimental data for binary benzene/n-hexane mixture.

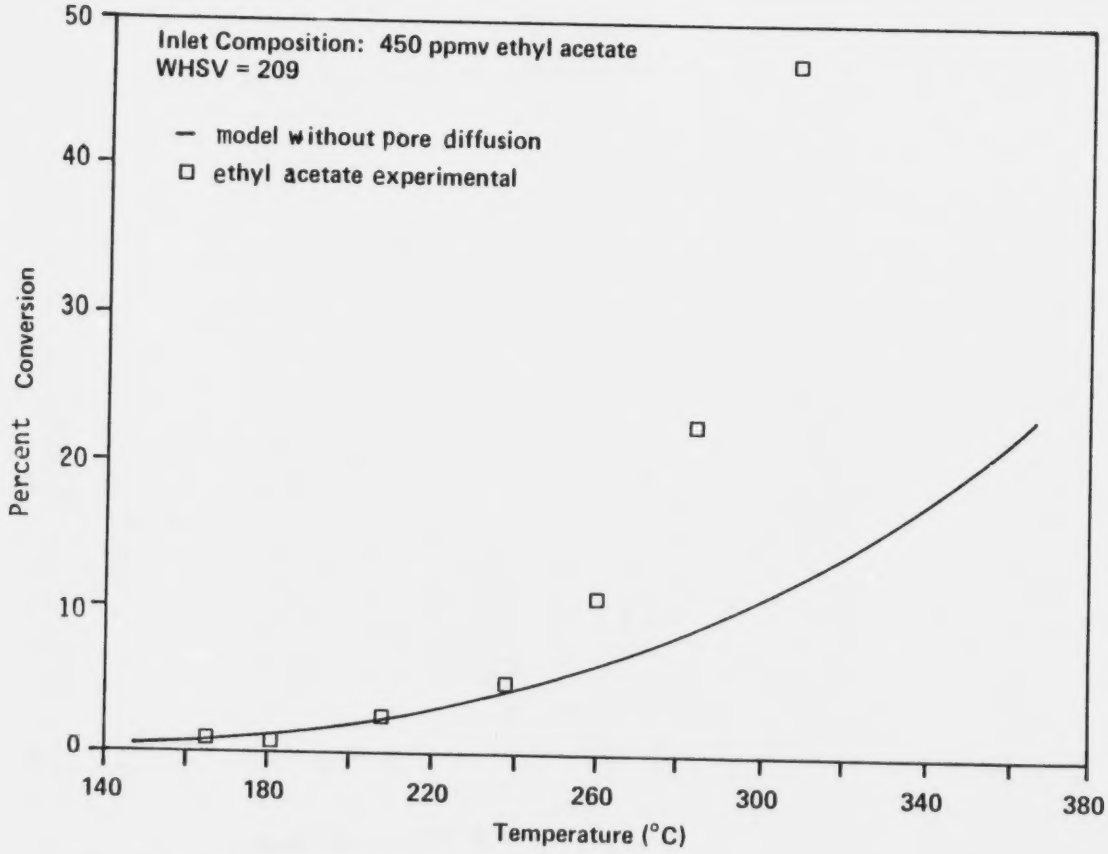

Figure 5-14. Comparison of model predictions and experimental data for ethyl acetate conversion as a single component.

simulations indicated the absence of pore diffusion hinderances in the 120 to 170 mesh particles, but the model is believed to be necessary for layer particles typical of industrial reactors. The model may also be extended to account for external diffusion effects. The Mars/van Krevelen kinetics reasonably simulate ethyl acetate oxidation at temperatures less than 220°C. Beyond 220°C, alternative reaction pathways such as thermal reactions (via free radical intermediates) may be present as seen from the much higher activation energy.

6.0 AUTOCATALYSIS IN DEEP OXIDATION OF ETHYL ACETATE

When the apparent order of a reaction shifts with increasing conversion, this suggests that the products of reaction are somehow speeding up the rate. Systems in which this occurs are often referred to as "autocatalytic". This may be represented in its simplest form for a second order reaction:

$$A + B \rightarrow B + B \qquad \text{where } r_A = kC_AC_B.$$

This implies, of course, that some of reactant B must be present for the reaction to proceed.

In principle the equations describing an autocatalytic reaction are simple; however, as noted earlier, these equations require an initial amount of compound B in order to be solved. The system under consideration here is a great deal more complex, in that a network of reactions contributes to the autocatalytic effect observed. Consider the homogeneous hydrolysis of ethyl acetate:

$$C_2H_3OOC_2H_5 + H_2O \rightarrow C_2H_3OOH + C_2H_5OH$$

Here, water must be present for the reaction to proceed to acetic acid and ethanol. This water may be present initially or generated during the combustion process:

$$C_2H_3OOC_2H_5 + 5O_2 \rightarrow 4CO_2 + 4H_2O$$

Essentially, once water (W) is initially formed in the reaction process, a mixture of ethyl acetate (EA), acetic acid (A) and ethanol (E) will be produced. It has been noted (Morrison and Boyd, 1974) that unlike hydrocarbons and alcohols with their uniform carbon-carbon linkages, esters with their oxygen linkages are comparatively unreactive compounds. Since this oxygen linkage is in fact quite stable towards oxidizing agents, attacks will preferentially occur at the electron deficient carbonyl carbon, resulting in the replacement of the $O-C_2H_5$ group by an electron rich moiety such as the

catalyst surface or a hydroxyl group. Combination with surface adsorbed oxygen is much less likely than hydrolysis at lower temperatures, and indeed, the presence of an acid catalyst makes the carbonyl even more susceptible to nucleophilic attack. The ethyl alcohol formed is substantially more reactive towards oxidation than the parent compound. Similarly, the presence of more reactive hydrocarbons such as benzene would also start and promote the hydrolysis/oxidation cycle. Thus, the reaction pathway for ethyl acetate oxidation would employ both homogeneous and heterogeneous steps. A general reaction scheme including carbon dioxide (C) and oxygen (O) may be written as follows:

$$EA + W \xrightarrow{k_1} A + E$$

$$EA + O \xrightarrow{k_2} W + C$$

$$A + O \xrightarrow{k_3} W + C$$

$$E + O \xrightarrow{k_4} W + C$$

If the relative value of the rate constant k_1 is greater than k_2 hydrolysis would be the original mechanism for decomposition and the sequential autocatalytic mechanism holds. The methodology for confirming this mechanism is fairly straight forward - merely humidify the inlet stream. The integral reactor results for a dry and humidified ethyl acetate stream are shown in Figure 6-1. A very clear enhancement is seen for all except the highest and lowest temperatures. For temperatures between 200°C and 260°C, the total conversion is more than doubled. These results would indicate that a hydrolysis mechanism is the most logical explanation for the "enhancement" phenomena observed earlier in the mixture tests. For example, with a reactive compound such as benzene:

$$C_6H_6 + 7.5O_2 \xrightarrow{k_5} 6CO_2 + 3H_2O$$

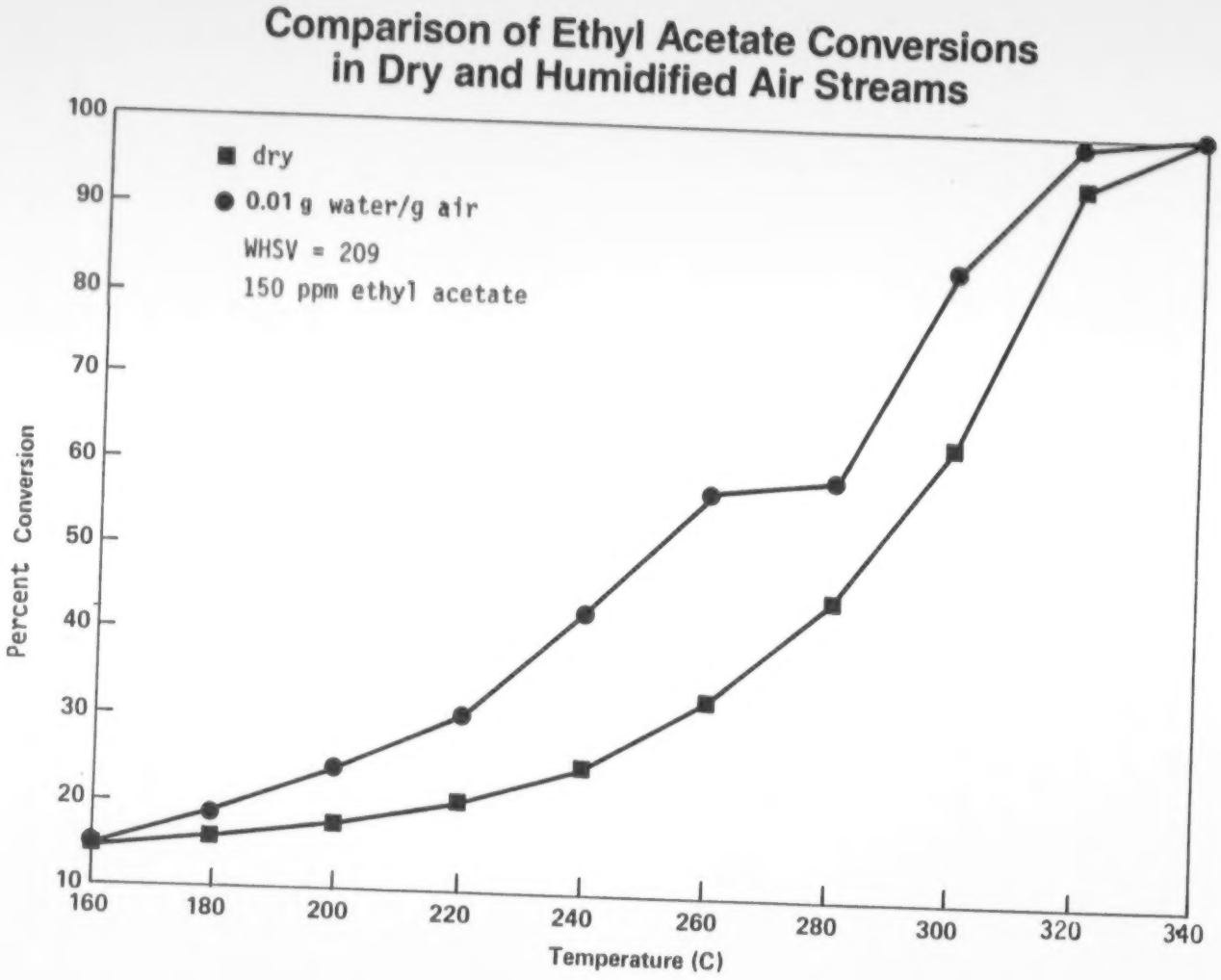

Figure 6-1. Comparison of ethyl acetate conversions in dry and humidified air streams.

three moles of water are produced per mole of benzene. Since we know from single component experiments that benzene oxidizes at substantially lower temperatures than ethyl acetate, water would be available for the hydrolysis reaction to occur at lower temperatures than with ethyl acetate alone. This mixed homogeneous/heterogeneous mechanism would also be consistent with the observation of the enhancement over different catalyst formulations used by Tichenor and Palazzolo (1987).

In the absence of detailed information on the water concentrations during the mixed oxidation reactions, one can still propose a kinetic expression for the hydrolysis/oxidation of ethyl acetate based upon several assumptions. First, that the hydrolysis step is the rate limiting step in ethyl acetate destruction. Second, that the contribution of water from the most reactive compound is most responsible for low-temperature enhancement. Finally, that the benzene rate expression is insensitive to mixture effects. Here, the rate of water production may be directly related to the benzene destruction:

$$\frac{r_{H_2O}}{3} = -r_{C_6H_6} = \frac{k_{O_{C_6H_6}} k_{C_6H_6} P_{C_6H_6} P_{O_2}}{k_{O_{C_6H_6}} P_{O_2} + \gamma_{C_6H_6} k_{C_6H_6} P_{C_6H_6}}$$

At steady state, the production of water from benzene oxidation is constant, and may be used in the expression for the homogeneous rate of hydrolysis of ethyl acetate:

$$r_{EA} = k\, C_{EA}\, C_W$$

Although this kinetic approach has merit, several other experiments should be used to confirm this mechanism.

- First, since the hydrolysis reaction is first order in water, the rate of reaction should be proportional to the water concentration in the inlet gas (for a differential reactor) up to the equilibrium limit.

- Second, the hydrolysis rate could be measured independently in a plug flow reactor without catalyst present. This rate could be compared to the rate of complete oxidation of ethyl acetate over a catalyst with and without water present.

- Thirdly, for mixtures the rate of ethyl acetate oxidation could be examined as a function of the water concentrations produced during the deep oxidation of the hydrocarbon mixtures. For example, in

mixtures of benzene and ethyl acetate one would predict the rate of ethyl acetate destruction to be directly proportional to the rate of benzene combustion. Similarly, the n-hexane/ethyl acetate mixtures the rate should be proportional to the rate of n-hexane combustion. Since the reactivity of n-hexane is lower than that of benzene, the "enhancement" should be less, and that is indeed what is observed for those binary mixtures. If sufficient information on the water concentrations produced in those tests exists, the mechanism could be confirmed quantitatively.

- Finally, the phenomenon of "auto-catalysis" may explain the inflection point in the first order Arrhenius plots noted for ethyl acetate much earlier in this study. Froment and Bishoff (1979) allude to such inflection points occurring with increasing conversion, so it may be worthwhile analyzing the results using this approach. Autocatalysis usually only becomes noticeable at conversions greater than ten percent. Once this mechanism becomes dominant, a distinct increase in activation energy should be noted for the reaction.

Water vapor seems to have only a minimal effect on the other oxygenated hydrocarbon, methyl ethyl ketone (MEK). As seen in Figure 6-2, some deviations between the humidified and dry stream reaction rates occur at temperatures below 240°C. At higher temperatures where autocatalysis should cause the largest deviation, the results match very closely. The suppressed rate below 180°C may be due to competitive adsorption of water on the catalyst, but clearly a different mechanism is in operation. This difference is not surprising, because MEK does not contain an ester linkage that may hydrolyze. Obviously, the mere presence of oxygen within a reactant is not nearly as important as the structure of the compound in determining the overall reaction rate for oxidation.

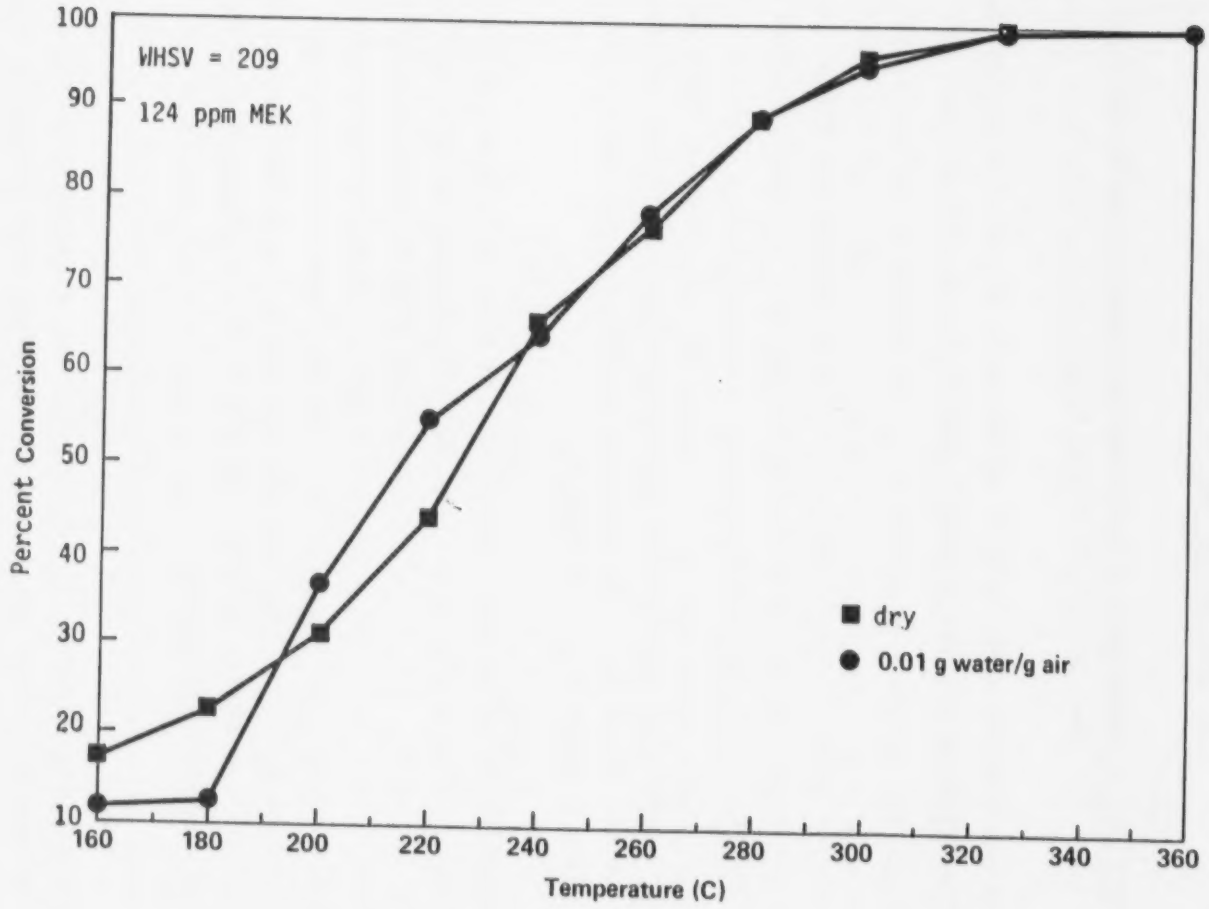

Figure 6-2. Comparison of MEK conversions in dry and humidified air streams.

7.0 CONCLUSIONS AND RECOMMENDATIONS

• Conversions of components in a mixture of organics may be significantly higher or lower than when present by themselves.

• Mars/van Krevelen (MVK) kinetic mechanism is an adequate representation for the deep oxidation of single organic compounds over the catalyst used in this study.

• A reactor model incorporating pore diffusion effects and MVK kinetics adequately explained single component benzene data over the entire temperature range of interest (150°C to 360°C).

• A multicomponent reactor model incorporating pore diffusion effects and a simple proposed extension of MVK kinetics was marginally successful in predicting benzene - n-hexane mixture behavior.

• Conversions of oxygenated species such as ethyl acetate are higher in mixtures than in single components. The MVK model appears to explain the data in the kinetic regime. MEK oxidation shows lower apparent enhancement than ethyl acetate. Other reaction pathways, including thermally enhanced free radical mechanisms and the interactions of oxygen containing species with partially reduced metal surfaces, may explain the observed phenomena. Further experimentation is necessary before a specific model can be postulated for the oxidation of oxygenated compounds.

• The presence of water vapor in the gas stream increases the conversion of ethyl acetate significantly. This suggests that autocatalysis by product water may be responsible for the observed enhancement described above. The fact that MEK conversions are not significantly affected by the presence of water vapor lends credence to this theory.

8.0 DATA QUALITY

The experiments were conducted in accordance with an approved draft of a quality assurance project plan.

8.1 Precision

All experiments involved sequential injections of reactor inlet and outlet to the gas chromatograph. The average of eight to ten injections was taken as the representative conversion for the conditions of each experiment. Since the inlet concentration was measured each time before measuring the outlet concentration, this gave eight to ten independent measurements of conversion for each experiment. This procedure also corrected for any drift in detector response over the course of the experiment. The calculated conversion is based on measured ratios of inlet to outlet peak areas. The relative percent deviation (RPD) may be calculated as

$$RPD = 100(ratio_{max} - ratio_{min})/ratio_{ave}$$

where $ratio_{max}$ is the maximum value of inlet to outlet peak areas, $ratio_{min}$ is the minimum value of inlet to outlet peak areas, and $ratio_{ave}$ is the average value of inlet to outlet peak areas for a given experiment.

Table 8-1 shows RPDs calculated for representative experiments with the four compounds studied. All values lie well within the quality assurance objective of 10 percent.

Gas flow rates were calibrated against a soap bubble flow meter at the beginning of each experiment and were not found to vary to any measurable exent during the course of the experiment.

Catalyst temperature was found to be reproducible to within 1 percent for a given controller setting.

8.2 Accuracy

All reported gas concentrations were referenced to standards certified by Scott Specialty Gases, Inc. against Standard Reference Materials (SRMs), which

TABLE 8-1. PRECISION OF DATA

Compound	Concentration	Temperature	Max. Ratio	Min. Ratio	Ave. Ratio	RPD (%)
Benzene	375 ppm	180°C	1.9165	1.893	1.9033	1.23
MEK	300 ppm	200°C	1.6988	1.654	1.6783	2.67
n-Hexane	410 ppm	280°C	2.9953	2.8458	2.9269	5.17
Ethyl Acetate	450 ppm	308°C	1.9014	1.8909	1.8947	0.55

are primary standards. Flame ionization detectors have responses that are linear in concentration, especially in the range of this study. This was verified in early experiments. Table 8-2 shows the bias in the concentrations reported by the vendor for uncertified tanks of MEK. In this case, the "true" value is that obtained by referencing against a certified tank of gas assuming linear FID response.

Gas flow rates were measured against a soap bubble flow meter, a primary standard, for each experiment.

Temperature measurements were referenced to an ice bath at 0°C.

8.3 Completeness

Since this was a laboratory study, all invalidated experiments could be repeated and all necessary experiments were performed.

8.4 External QA Audit

None was performed.

TABLE 8-2. ACCURACY OF DATA

Nominal Value (ppm)	True Value (ppm)(a)	Bias (%)
39	50.4	22.61
71.7	70.0	2.43
135	141.8	4.80
188.8	189.4	0.32
300.3	297.4	0.98

(a) Referenced against certified standard assuming linear FID response

9.0 NOMENCLATURE

			Units
C_i	=	hydrocarbon [VOC] concentration	[mol/cm^3]
C_{ik}	=	intraparticle concentration of species i	[mol/cm^3]
C_{i_o}	=	inlet hydrocarbon [VOC] concentration	[mol/cm^3]
C_o	=	oxygen concentration	[mol/cm^3]
$D_{eff(i)}$	=	effective diffusivity of species i	[cm^2/s]
$\bar{D}_{i\text{-}air}$	=	binary molecular diffusivity	[cm^2/s]
$(\bar{D}_k)_{Mi}$	=	macropore Knudsen diffusivity	[cm^2/s]
$(\bar{D}_k)_{ui}$	=	micropore Knudsen diffusivity	[cm^2/s]
$\bar{D}_{Mi}$	=	effective macropore diffusivity	[cm^2/s]
$\bar{D}_{ui}$	=	effective micropore diffusivity	[cm^2/s]
E	=	activation energy	[J/mol.K)]
f_i	=	fractional conversion of species i	(--)
h_i	=	Thiele modulii for species i $R_o\sqrt{\frac{k_i \rho_p}{D_{eff(i)}}}$	[--]
k_B	=	Boltzmann constant	
$k_{f(i)}$	=	mass transfer coefficient of species i	[cm/s]
K_{H_2O}	=	adsorption equilibrium constant for H_2O	[--]
k_i	=	surface reduction rate constant for species i	[cm^3/(g·s)]
K_i	=	$\gamma_i \left[\frac{k_i}{k_{o_i}}\right] \left[\frac{C_{io}}{C_o}\right]$	[--]
k_{o_i}	=	surface reoxidation rate constant for species i	[cm^3/(g·s)]
m_i	=	$(d\alpha_{ik}/dn)$	[--]

$(MW)_i$	=	molecular weight of species i	[--]
P	=	pressure	[atm]
R	=	particle radial coordinate	[cm]
$\bar{r}$	=	average pore radius	[cm]
r_i	=	rate of oxidation of species i	[mol/(g·s)]
R_i	=	hydrocarbon species, i	[--]
r_{ik}	=	intraparticle rate of reaction	[mol/(g·s)]
$\bar{r}_M$	=	average macropore radius	[cm]
R_o	=	particle radius	[cm]
$\bar{r}_u$	=	average micropore radius	[cm]
r_{O_2}	=	rate of oxygen consumption	[mol/(g·s)]
S_g	=	catalyst surface area	[cm^2/g]
t	=	temperature	[°C]
T	=	absolute temperature	[K]
v	=	volumetric flow rate at reaction temperature	[cm^3/s]
w	=	dimensionless catalyst weight in reactor	[g]
W	=	catalyst weight coordinate	[g]
W_F	=	total weight of catalyst in reactor	[g]
WHSV	=	weight hourly space velocity	[g gas/(g catalyst·h)]

GREEK NOMECLATURE

α_i	=	dimensionless bulk concentration, C_i/C_{io}	[--]
α_{ik}	=	dimensionless intraparticle concentration, C_{ik}/C_{io}	[--]
β	=	$k_i W_F/v$	[--]
ϵ	=	Lennard-Jones parameter	
ϵ_M	=	macropore void fraction	[--]

ε_μ	=	micropore void fraction	[--]
γ_i	=	stoichiometric coefficient for deep oxidation of species i	[--]
η	=	dimensionless particle radial coordinate, R/R_o	[--]
λ_i	=	$(3\ D_{eff(i)}\ W_F)/(vR_o^2\ \rho_p)$	[--]
ρ_p	=	particle density	[g/cm^3]
σ	=	Lennard-Jones parameter	
θ	=	fraction of oxidized catalyst	[--]
$\theta_1, \theta_2, \theta_3$	=	fraction of reduced catalyst corresponding to n-hexane, benzene, and ethyl acetate, respectively	[--]
$\Omega_{i\text{-}air}$	=	collision integral	

10.0 REFERENCES

Acres, G.J.K. 1970. Platinum Catalysts for the Control of Air Pollution Plat. Met. Rev. 14:2-10.

Balasubramanian, S. and D. S. Viswanath. 1975. Ind. Eng. Chem. Fundam., 14:3, p. 158.

Box, J. M. 1966. Comp. J. pp.67-77.

Cullis, C.F., D.E. Keene, and D.L. Trimm. 1970. Studies of the Partial Oxidation of Methane over Heterogeneous Catalysts. Journal of Catalysis 19:378-385.

Emmett, P.H. (ed.). 1960. Catalysis. Reinhold, New York.

Froment, G.F., and K.B. Bischoff. 1979. Chemical Reactor Analysis and Design. John Wiley and Sons.

Golodets, G. I. 1983. Heterogeneous Catalytic Reaction Involving Molecular Oxygen, Elsevier, New York, Part III, p. 396.

Hawthorn, R.D. 1974. Afterburner Catalysts - Effects of Heat and Mass Transfer Between Gas and Catalyst Surface, AIChE Symp. Serv., Recent Adv. Air Pol. Control, 70:137, p. 428.

Heyes, C.J., J.G. Irwin, H.A. Johnson, and R.L. Moss. 1982. The Catalytic Oxidation of Organic Air Pollutants, Part 2. Cobalt Molybdate and Copper Chromite Catalysts. J. Chem. Tech. Biotechnol. 32:1034-1041.

Hirschfelder, J. O., C. F. Curtiss, and R. B. Bird, "Molecular Theory of Gases and Liquids," pp.539, 578, John Wiley and Sons, Inc. NY.

Jaswal, I. S., R. F. Mann, J. A. Junsola, and J. Downie, 1969. Can. J. Chem. Eng., 47, p. 284.

Mars, P., and D. W. van Krevelen, 1954. Special Supplement to: Chem. Eng. Sci., 3, p 41.

Moro-Oka, Y., Y. Morihama, and A. Ozaki, 1967. J. Catal. 7:2.

Morrison, R.T., and R.N. Boyd, 1974. Organic Chemistry (3rd ed.), Allyn and Bacon, Inc.

Palazzolo, M. A., J. I. Steinmetz, D. L. Lewis, and J. F. Beltz, 1985. Parametric Evaluation of VOC/HAP Destruction Via Catalytic Incineration. Report No. EPA-600/2-85-041 (NTIS No. PB85-191187/A7). U.S. Environmental Protection Agency.

Pope, D., D.S. Walker, and R.L. Moss. 1976. Evaluation of Cobalt Oxide Catalysts for the Oxidation of Low Concentrations of Organic Compounds in Air. Atmospheric Environment 10:951-956.

Prasad, R., L.A. Kennedy, and E. Ruckenstein. 1984. Catalytic Combustion. Catal. Rev. Sci. Eng. 26(1):1-58.

Sadamori, H., A. Chikazawa, S. Okamura, and T. Noda. 1981. Development of Low Temperature Catalytic Burner. Gas Research Conference. Gas Research Institute, p. 1467.

Satterfield, C.N. 1980. Heterogeneous Catalysis in Practice. McGraw-Hill, New York.

Smith, J. M. 1981. Chem. Eng. Kinetics, 3rd ed., p.455, McGraw-Hill, NY

Spivey, J.J. 1987. Complete Catalytic Oxidation of Volatile Organics. I & EC Res., (in press).

Tichenor, B. A. and M. A. Palazzolo, 1987. Destruction of Volatile Organic Compounds via Catalytic Incineration, Environmental Progress, 6(3), 172-176.

Wakao, N. and J. M. Smith, 1962. Chem. Eng. Sci., 17, p. 825.

Yao, Y.F.Y. 1973. The Oxidation of Hydrocarbons and CO Over Metal Oxides: II. α-Cr_2O_3. Journal of Catalysis 28:139-149.